Catalysis Science & Technology

MINIREVIEW

View Article Online
View Journal | View Issue

Cite this: *Catal. Sci. Technol.*, 2017, 7, 4905

Recent advances of the nano-hierarchical SAPO-34 in the methanol-to-olefin (MTO) reaction and other applications

Jiawei Zhong,[abd] Jingfeng Han,[a] Yingxu Wei,*[a] Peng Tian,[a] Xinwen Guo,[b] Chunshan Song[be] and Zhongmin Liu*[ac]

Received 20th July 2017,
Accepted 15th September 2017

DOI: 10.1039/c7cy01466j

rsc.li/catalysis

The recent advances in synthesis and catalytic applications of nano-hierarchical SAPO-34 for methanol-to-olefin (MTO) conversion and other reactions have been elaborated in this minireview. The structure, unique properties (*e.g.*, shape selectivity), and diffusion of zeolites and molecular sieves are briefly covered in the first part. An overview of the development of synthetic methods for the preparation of nanosized SAPO-34 and hierarchical SAPO-34 is included in the second and third parts, with focus on the novel and green preparation strategies. The advantages and disadvantages of the different synthetic approaches are discussed in detail, and the relationship between the catalytic performance and the diffusion and acidity is also elucidated. Finally, the updated characterization techniques considering the interconnectivity between the pore channels are outlined.

1. Introduction

Zeolites are crystalline, microporous aluminosilicates composed of tetrahedral building units TO_4 (T = Al or Si) connected with corner-sharing oxygen atoms, forming three-dimensional frameworks with well-defined channels or cavities of molecular dimensions. Molecular sieves, the so-called zeotype materials or zeolitic molecular sieves (ZMSs), are also a promising class of inorganic porous materials containing a variety of tetrahedral ($T_{1/4}$ = Si, P, Al, Ti, Ga, Ge, B, *etc.*) framework cations.[1,2] According to the International Zeolite Association (IZA), to date, approximately 232 framework type codes (*e.g.*, CHA, MFI, FAU and MOR) have been identified and confirmed.[3,4]

In general, zeolites and molecular sieves possess well-defined micropores of molecular dimensions, typically in the 0.4–1.2 nm range. The micropores can be further classified into 8-, 10- and 12-membered ring pore openings, corresponding to pore widths of approximately 0.4 nm, 0.55 nm and 0.7 nm. Therefore, shape selectivity, a unique molecular sieving property, effectively discriminates zeolites and molecular sieves from other porous materials.[5–7] In particular, shape selectivity can be categorised into reactant shape selectivity, product shape selectivity and transition-state shape selectivity (Fig. 1). For reactant selectivity, bulky components in the feedstock larger than the pore entrance are unable to access the catalytically active sites inside the pore channels. In the case of transition state selectivity, the geometrical constraints within the pore channel inhibit the formation of the

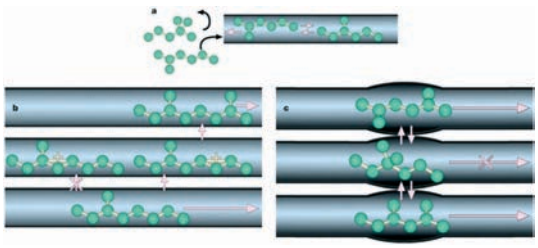

Fig. 1 Shape selectivity in molecular sieves. (a) Reactant shape selectivity: molecules larger than the pore entrance cannot reach acid sites and are unable to convert to products. (b) Transition-state shape selectivity: transition states that are too bulky to fit inside a pore do not form. (c) Product shape selectivity: molecules formed in the adsorbed phase are too large to desorb as products (reproduced with permission from ref. 8). Copyright © 2008, Rights Managed by Nature Publishing Group.[8]

[a] *National Engineering Laboratory for Methanol to Olefins, State Energy Low Carbon Catalysis and Engineering R&D Center, Dalian National Laboratory for Clean Energy, iChEM (Collaborative Innovation Center of Chemistry for Energy Materials), Dalian Institute of Chemical Physics, Chinese Academy of Sciences, Dalian 116023, PR China. E-mail: liuzm@dicp.ac.cn, weiyx@dicp.ac.cn; Fax: +86 411 84691570; Tel: +86 411 84379335*
[b] *State Key Laboratory of Fine Chemicals, PSU-DUT Joint Center for Energy Research, School of Chemical Engineering, Dalian University of Technology, Dalian 116024, PR China*
[c] *State Key Laboratory of Catalysis, Dalian Institute of Chemical Physics, Chinese Academy of Sciences, Dalian 116023, PR China*
[d] *University of Chinese Academy of Sciences, Beijing 100049, PR China*
[e] *Departments of Energy and Mineral Engineering and of Chemical Engineering, EMS Energy Institute, The Pennsylvania State University, University Park, PA 16802, USA*

transition states leading to the formation of certain products. As for the product selectivity, only those products with suitable molecular dimensions are able to diffuse out of the crystals, while those with too large size cannot diffuse out or only diffuse slowly as products.

The excellent flexibility in the structure type and chemical composition results in tuneable chemical properties of zeolites and molecular sieves. Attributed to the well-defined micropore sizes for molecular shape selectivity, appropriate acidity, large specific surface areas, and high chemical and physical (*e.g.*, hydrothermal, thermal and mechanical) stability, at present, zeolites and molecular sieves exert significant impacts on the modern society, and are applied in a wide variety of advanced industrial processes related to detergency, gas adsorption and separation as well as catalysis.[9,10] For instance, zeolites and molecular sieves act as water softeners to remove the undesired Mg^{2+} and Ca^{2+} ions from water with high mineral content. Moreover, zeolites and molecular sieves can be used in gas phase adsorptive separation (*e.g.* adsorbents for CO_2 removal from CH_4 or N_2). In addition, zeolites and molecular sieves can be adopted to selectively reduce the NO_x in vehicle exhaust gases. In particular, zeolites and molecular sieves, as efficient heterogeneous catalysts, exhibit kaleidoscopic applications in petroleum refining and petro-chemical processes.[9,10] For example, fluid catalytic cracking (FCC) and hydro-cracking (HC) are typical commercialized industrial processes. Likewise, zeolite/molecular sieve-based catalytic technologies include the Friedel–Crafts

Jiawei Zhong

Jiawei Zhong completed a graduate course at the University of Science and Technology of China (USTC) in 2013, joined Guangzhou Institute of Energy Conversion (GIEC) and received his M.S. from the University of Chinese Academy of Sciences (UCAS) in 2015. He gave up the opportunity to join Eindhoven University of Technology (TU/e) with financial support from the China Scholarship Council, and joined Dalian National Laboratory for Clean Energy (DNL), Dalian Institute of Chemical Physics (DICP), Chinese Academy of Sciences (CAS). He is pursuing his Ph.D. from Dalian University of Technology (DUT). His research interests include methanol to olefin conversion and the catalytic conversion of biomass into chemicals.

Yingxu Wei

Yingxu Wei received her PhD at Dalian Institute of Chemical Physics (DICP), Chinese Academy of Sciences (CAS) in 2001. She conducted postdoctoral study at the University of Namur (Belgium) from 2003 to 2004. She has been the group leader of Catalysis and New Catalytic Reactions in the National Engineering Laboratory of Methanol to Olefins since 2009 and was promoted to professor in 2011. Prof. Wei has undertaken a number of projects commissioned by the NSFC, CAS and PetroChina. She has been involved in research on heterogeneous catalysis and methanol to olefin conversion. Over 70 academic papers authored by Prof. Wei have been published and more than 30 patents have been granted.

Peng Tian

Peng Tian obtained her PhD from Dalian Institute of Chemical Physics, CAS, in 2004. Currently, she is a professor and team leader of molecular sieves synthesis at Dalian Institute of Chemical Physics. In 2016, she received the "Qiushi Outstanding Youth Award" for transformation of scientific and technological achievements (China). Her main research interests include synthesis and catalytic application of molecular sieve materials, methanol conversion and NH_3-SCR reaction.

Xinwen Guo

Professor Xinwen Guo received his Ph.D. degree in Industrial Catalysis from Dalian University of Technology (DUT), in 1994, and was promoted to full professor in 2001. From 2001 to 2002, he was a visiting Professor at Penn State University. He is now the Vice Dean of the Faculty of Chemical, Environmental and Biological Science and Technology, DUT. His research interests are mainly focused on the catalytic conversion of carbon dioxide and molecular sieve catalysis. He has published more than 260 peer-reviewed papers and 30 patents. He is an Editorial Board Member of the Chinese Journal of Catalysis, Chemical Engineering and Technology.

alkylation, isomerization, dewaxing and reforming. In the past decades, methanol-to-hydrocarbons (MTH) technology for the production of light olefins, gasoline and aromatics has attracted considerable academic and commercial interest due to the ever-increasing oil price. The methanol-to-olefin (MTO) reaction, in particular, is of growing industrial significance in the past years in China with the emergence of the new coal chemical industry.[11]

It is worth stressing that the catalytic performances strongly correlate with the accessibility of the catalytically active sites, which is affected by pore size and pore connectivity. Internal diffusion limitations within the pores can result in severe disadvantages such as pore blocking, retarded mass transport and coke formation. It is widely accepted that the intracrystalline mass transport from and/or to the active sites inside the micropores (configurational diffusion) is considerably slower than its counterparts (molecular diffusion and Knudsen diffusion) (Fig. 2), resulting in a fast deactivation rate.[12] Therefore, up to now, considerable effort has been devoted to alleviating the diffusion limitations.

The degree of catalyst utilization is classically described by the effectiveness factor η (Fig. 3). Free of any diffusion constraints, in particular, full utilization of the catalyst particle ($\eta \rightarrow 1$) takes place at low values of the Thiele modulus ($\varphi \rightarrow 0$). On the contrary, $\varphi = 10$ renders $\eta = 0.1$, meaning that only 10% of the catalyst surface is utilized. The Thiele modulus (φ) is calculated from the characteristic length for diffusion (L), the intrinsic reaction rate constant (k), and the effective diffusivity (D_{eff}). Since the intrinsic rate coefficient k is fixed for a given reaction and molecular sieve, shortening the diffusion length L and/or enhancing the effective diffusivity D_{eff} in the pores substantially decreases the Thiele modulus.[14]

There are mainly three strategies to shorten the intracrystalline diffusion path length, the reduction of the crystal size (*e.g.*, the nano-sized zeolite route), hierarchization (the incorporation of an auxiliary pore-structure other than the intrinsic microporous structure) or the combination of both strategies (Fig. 4).

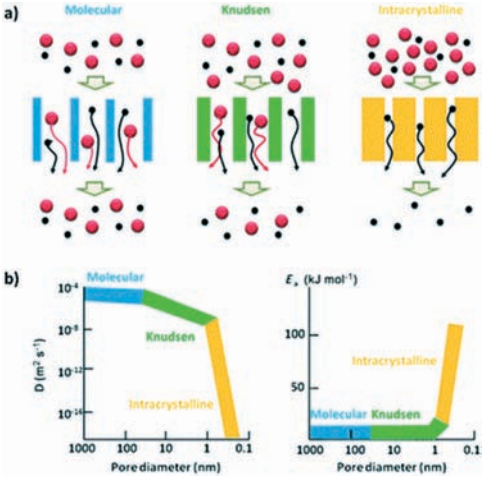

Fig. 2 (a) The diffusion of large (red) and small (black) molecules within macropores (blue), mesopores (green) and micropores (yellow). (b) The diffusion coefficients (D) and activation energy (E_a) in diffusion regimes. Figure reproduced from ref. 13 with permission from Wiley-VCH.[13]

The nanosized and hierarchical zeolites and molecular sieves effectively decrease the intracrystalline diffusion path length, greatly enhance the mass flow to and away from the catalytic centres, overcome the diffusion limitation, and subsequently accelerate catalytic conversion, prohibit the undesired secondary reaction, reduce coke formation and prolong the catalyst lifetime. In particular, the hierarchical zeolites and molecular sieves, just like a metropolis consisting of both narrow pathways and broad streets

Chunshan Song

Chunshan Song is a Distinguished Professor of Fuel Science and Chemical Engineering and Director of EMS Energy Institute at the Pennsylvania State University. He is also the Director of the Joint Center for Energy Research between Penn State and Dalian University of Technology where he is a ChangJiang Scholar and QianRen Professor. His research focuses on catalysis and catalytic materials for clean fuels and chemicals, shape-selective synthesis, and CO_2 capture and utilization. He has 340 refereed publications, and has received many awards such as the Henry Storch Award, ACS Fellow, Distinguished Fulbright Scholar and Herman Pines Award. He is the Editor for Advances in Catalysis.

Zhongmin Liu

Professor Zhongmin Liu has been the Director of Dalian Institute of Chemical Physics, CAS since 2017. In 2006, as a leading scientist, Professor Liu successfully accomplished the industrial demonstration test of DMTO technology. Based on DMTO technology, the world's first commercial MTO unit was built by Shenhua group, which was a milestone for coal to chemicals. He has published more than 300 papers, and has applied for more than 600 patents. He is a member of the International Academic Committee of the 13th, 14th and 17th International Zeolite Conference. He has received many awards such as the National Technological Invention Awards First Prize of China (2014), and the Science and Technology Innovation Award of the HLHL Foundation (2015). He was elected academician of the Chinese Academy of Engineering in 2015.

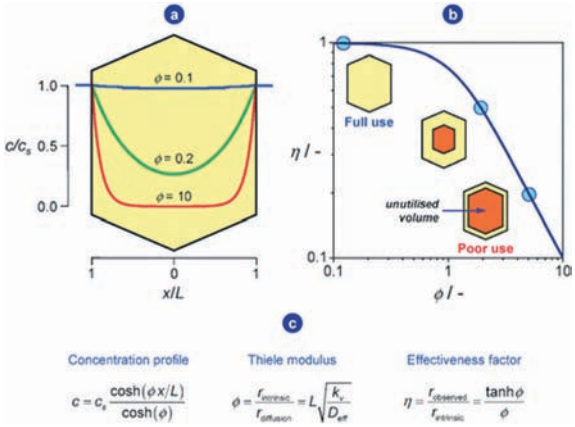

Fig. 3 (a) The concentration profiles across a zeolite crystal at different values of the Thiele modulus (φ). The reactant concentration across a zeolite crystal is exhausted ($c/c_s = 0$) near the surface at φ = 10, while being practically uniform and very similar to the surface concentration ($c/c_s = 1$) at $\varphi = 0.1$. (b) Dependence of the effectiveness factor (η) on the Thiele modulus (φ). A high Thiele modulus renders a catalyst poorly utilized ($\varphi \rightarrow \infty$, $\eta \rightarrow 1/\varphi$). Reproduced from ref. 15 with permission from The Royal Society of Chemistry.[15] Relevant equations to construct the graphs (a) and (b) are given in (c).

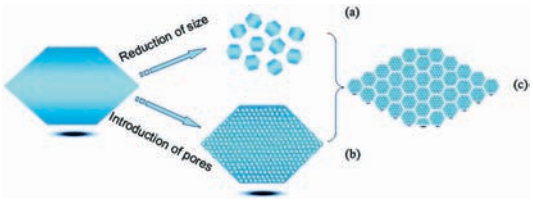

Fig. 4 The strategies to shorten the diffusion path length and increase the external surface area: (a) downsizing the crystals, (b) introduction of additional pores and (c) decrease of size and introduction of auxiliary pores in nanosized crystals. Reproduced from ref. 16 with permission from The Royal Society of Chemistry.[16]

(Fig. 5), besides exhibiting all the benefits mentioned above, also enable the processing of molecules that exceed the size of micropores, with the similar function of extra-large-pore molecular sieves,[17] and have drawn significant attention. The hierarchically porous zeolites and molecular sieves contain additional mesopores (pores with diameters ranging between 2 and 50 nm) and/or macropores (pores with diameters >50 nm). In particular, the introduced mesopores can be categorized into intra- or inter-crystalline mesopores. Inter-crystalline mesopores are the voids originating from crystal aggregation, whereas intra-crystalline mesopores are generated within the zeolites and zeotype materials. In other words, the inter-crystalline mesopores occur in the vicinity of the crystallite surface while the intra-crystalline mesopores are located inside the crystal.

Fig. 5 (a) The conventional microporous molecular sieves (crowded streets). (b) and (c) The hierarchical molecular sieves with interconnected networks of micropores (narrow streets) and meso–macropores (broader streets). Caption reproduced with permission from ref. 23. Copyright © 2012, Rights Managed by Nature Publishing Group.[23]

In general, the synthetic strategies towards hierarchical zeolites and molecular sieves can be categorized into "top-down" or "bottom-up" methods. On one hand, the top-down approach, an *ex situ* post-synthetic demetallation method, includes preferential element extraction from the framework such as dealumination by acids and desilication by inorganic bases or organic amines.[18] On the other hand, the bottom-up approach, an *in situ* templating method, can be further classified into hard- or soft-template methods. The hard-template method commonly employs solid structures which usually do not react in synthesis medium, like carbonaceous materials, organic aerogels, biological templates and so on, to name just a few. As for the soft-template method, soft templates which react with other ingredients in synthesis medium, including long-chained polymers, amphiphilic organosilanes, and supramolecular cationic surfactants with flexible structures, have been utilized for the generation of auxiliary mesoporosity.[19–22]

There is no doubt that the nanosized and hierarchical zeolites and molecular sieves show considerable advantages in the micropore reaction (the reactions occurred within the micropore), external surface reaction (the reactions catalysed at the external surface) and shape-selective reaction (the reactions exhibit shape selectivity) (Fig. 6).[24] In particular, owing to the ever-increasing demand for light olefins and the limited reserve of crude oil, the past few years have witnessed the rapid development of methanol-to-olefin (MTO) conversion, an alternative route for the production of light olefins from non-oil sources in a post-oil society. Methanol is commonly produced from the reaction of synthesis gas obtained by gasification of fossil carbon sources or steam-reforming of natural gas. It is believed that the ever-growing exploitation

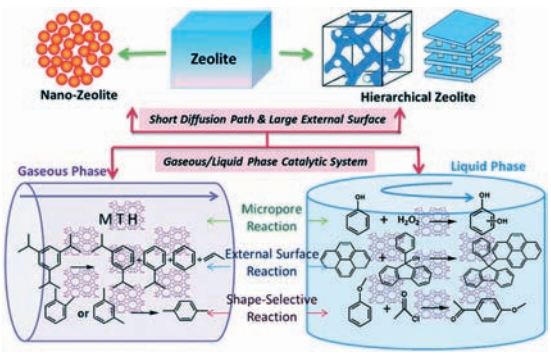

Fig. 6 Structure characteristics and catalytic applications of nanosized/hierarchical zeolites in gaseous/liquid phase reactions. Caption reproduced from ref. 24 with permission from The Royal Society of Chemistry.[24]

of shale gas will definitely lead to more economical production of methane. Furthermore, it might be an environmentally friendly carbon-neutral route if the methanol were produced by chemical recycling of carbon dioxide *via* hydrogenation or from synthesis gas obtained by gasification of renewable biomass. Due to the contribution of the CHA topological structure with a large cavity (9.4 Å in diameter) and small 8-ring pore (3.8 Å × 3.8 Å), moderate acidity, and high hydrothermal stability, the zeolite-type microporous silicoaluminophosphate SAPO-34 exhibited excellent performance in the methanol-to-olefin (MTO) reaction, achieving exceptionally high selectivity towards light olefins (typically above 80%).[25] Nevertheless, SAPO-34 suffers from rapid deactivation owing to retained organic species in the large CHA cavity. It has been demonstrated that the catalytic performance, especially the deactivation behaviour in the MTO reaction, is strongly related to the diffusion limitation.[26] Therefore, nanosized SAPO-34 shows slower deactivation due to the higher proportion of accessible cages near the external surface. Likewise, hierarchical SAPO-34 also exhibits excellent catalytic performance owing to the alleviated diffusion limitation.

There are a plethora of comprehensive reviews and books concerning the synthetic approaches for hierarchical zeolites[27–32] and nanosized zeolites.[16,33,34] However, the majority are focused on the preparation of aluminosilicate zeolites. Since the synthetic strategies towards nanosized and hierarchical SAPO-type molecular sieves are not identical to those towards aluminosilicate zeolites, the synthesis of nanosized and hierarchical SAPO-type materials should be clearly illustrated. Likewise, the recent progress of the methanol-to-olefin (MTO) reaction has also been summarized in a wealth of book chapters,[35–39] with the major emphasis on the hydrocarbon pool mechanism or its industrial application. Nevertheless, less attention is paid to the application of nanosized and hierarchical molecular sieves in the MTO reaction. The main purpose of this minireview is, therefore, to elaborate on the recent development of nano-hierarchical SAPO-34 in MTO conversion. The associated advantages and disadvantages of the different synthetic approaches will be discussed, with emphasis on the novel synthesis strategies and the relationship between the catalytic performance and diffusion and acidity.

2. Synthesis of nanosized SAPO-34

In general, the reduction of crystal size results in increased external surface area and shortened diffusion path length, which facilitates mass transfer and alleviates the diffusion limitation in catalytic reactions. Moreover, smaller particle size enhances catalytic performance by dramatically suppressing the side reactions such as coke deposition. Specifically, it is widely acknowledged that the number of accessible cages near the external surface of SAPO-34 plays a tremendous role in the MTO conversion,[26] and decreasing the crystal size of SAPO-34 results in a larger proportion of accessible cages, which is beneficial for the enhancement of catalyst lifetime. The synthesis of nanosized SAPO-34 was usually achieved by optimizing the reaction parameters to increase the number of nuclei and to reduce the crystal growth rate, namely, accelerate nucleation over crystal growth (*e.g.*, low crystallization temperature, aging, high alkalinity, high solubility of the silica source).[40] Nevertheless, it is worth underlining that the synthesis of nanostructured molecular sieves is of great challenge. The crystallization of zeolites and molecular sieves is usually accompanied by Ostwald ripening, a process that minimizes the surface free energy of crystals, leading to the dissolution of smaller crystals and their further growth into larger crystals.[41] Therefore, in this section, not only nanostructured molecular sieves (1–100 nm) but also submicrometer-sized molecular sieves with a size of less than 1000 nm are included. Besides, the approaches such as microwave synthesis, dry gel conversion, ultrasound-assisted synthesis, fast high-temperature synthesis, and multi-template synthesis will be just briefly addressed since these methods have been substantially reviewed by some research groups.[42,43]

2.1 Microwave synthesis

Compared with conventional hydrothermal synthesis, the microwave heating technique, as a green and energy-efficient way of heating, has the following advantages.[34,44–46] Firstly, microwave irradiation enhances the heating rate and the substrate mixture can achieve the desired temperature rapidly, which substantially shorten the crystallization time of nanoporous molecular sieves. Moreover, microwave irradiation results in more homogeneous heating, which avoids the undesirable temperature gradient encountered during conventional hydrothermal synthesis. Additionally, microwave energy enhances the rate of the dissolution of the precursor gel. Therefore, the microwave heating technique has been regarded as an effective way to synthesize defect-free, uniform and small-sized crystals due to the high concentration of nuclei and accelerated homogeneous nucleation through rapid and uniform heating.

Bein *et al.* first prepared cube-like SAPO-34 with an average crystal size of 206 nm with colloidal silica as the silica source and tetraethylammonium hydroxide (TEAOH) as the template under microwave conditions, with the majority exhibiting diameters of about 100 nm.[47] Park *et al.* noted that the increase of crystallization time under microwave irradiation is beneficial for the transformation of SAPO-5 with a relatively unstable AFI structure formed at the early stage into more stable SAPO-34.[48] Likewise, Jhung and coworkers systematically investigated the preparation conditions including crystallization temperature and time as well as template and silica source content under microwave heating. They came to the conclusion that high concentrations of TEAOH and the silica source and high reaction temperatures are beneficial for the formation of SAPO-34 rather than SAPO-5. Small-sized and uniform SAPO-34 crystals (<0.2 μm) are obtained and SAPO-34 can be obtained rapidly within 5 min under 210 °C

with the TEAOH template.[49] Similarly, Carreon prepared uniform SAPO-34 with about 500 nm size through the phase transformation of SAPO-5 under microwave heating, and investigated its performance in the selective adsorption of CO_2 from CH_4.[50] However, dual TEAOH and dipropylamine (DPA) templates are adopted and pure SAPO-34 is obtained only after quite a long time (500 min).

Yu and co-workers have carried out extensive work on the impact of synthetic factors, such as the silica source, water content, crystallization time and aging time, on the morphology of SAPO-34 under microwave irradiation.[51] It is observed that sheet-like nanocrystals (250 × 50 nm) change to nanoparticles with a diameter of about 100 nm by changing colloidal silica to TEOS, and nanoparticles with sizes of 60–80 nm can be obtained when the aging time is prolonged to 60 h. Moreover, their group demonstrated that sheet-like SAPO-34 with a size of 20 × 250 × 250 nm and nanospherical SAPO-34 with a size of 80 nm can be synthesized under optimized conditions though colloidal silica and TEOS, respectively.[52] On one hand, the large external surfaces enhance exposure of catalytically active sites to the reactants, which guarantees the high catalytic activity. On the other hand, the decreased crystal size remarkably facilitates the mass flow of products, inhibits the hydrogen-transfer reaction between olefin products and confined aromatics such as methylbenzenes and methylnaphthalenes, and depresses the formation of polycyclic aromatics, which results in an enhanced catalyst lifespan and a low coking rate (Fig. 7).

Márquez-Álvarez and coworkers prepared nanoplate-like SAPO-34 with a thickness of a few tenths of nanometers from highly diluted precursor solutions with aluminium chloride in a microwave environment.[53,54] It is observed that the microwave-assisted synthesis with Ludox or TEOS results in a lower incorporated silicon amount and subsequently reduced acidity. Furthermore, the thin plate-like structure facilitates the accessibility of the reactants to the acid sites, shortens the diffusion path, and decreases the residence time of the reactants and products inside the micropores, which result in longer catalyst lifetime in the MTO reaction. Sun and coworkers also investigated in great detail the influence of organic templates, crystallization time and temperature on the crystal morphology, and prepared nanosheet-like SAPO-34 with a size of about 1000 × 1000 × 130 nm at 220 °C for 2 h with a TEAOH template under microwave conditions.[55,56] The sheet-like SAPO-34 exhibits a catalyst lifetime of 380 min, and provides an ethylene selectivity of 51.7% and a total selectivity for C2–C4 olefins of 90.2% under 450 °C with a volume hourly space velocity of 1.0 h^{-1}. It is proposed that the use of microwaves leads to high nucleation density and a slow crystal growth rate, which results in the unique morphology of the sheet-like nano-SAPO-34. The sheet-like nanostructures shorten the diffusion path and decrease the coke formation rate, which result in longer stability and higher olefin selectivity. Halladj *et al.* synthesized nanosized SAPO-34 crystals through microwave-assisted hydrothermal synthesis.[57] It is found that contributing factors such as microwave power delivery and microwave irradiation time have great impact on the size and morphology of the crystals.

Corma synthesized spherical nano-SAPO-34 with 150–300 nm size aggregated from smaller crystals of 20–50 nm under microwave heating and investigated the stability of nano-SAPO-34 under moisture.[58] It is found that selective hydrolysis of the Si–O–Al groups on the edge of the silicon islands, the acid sites that are associated with higher acidity and favor coking and deactivation, firstly occurs, which results in decreased overall acidity, lower deactivation rates and longer catalyst lifetime. However, the continued hydrolysis of both Si–O–Al and Al–O–P bonds after 14 days decreases the catalyst lifetime. Since silicon at the border of the silicon islands with higher acid strength induces higher C2/C3 ratios, therefore, the exposure to moisture results in a decreased C2/C3 ratio. Nevertheless, the low yield of nanosized SAPO-34 prepared from the microwave-assisted method (*e.g.*, 15%) limits its large-scale industrial application.

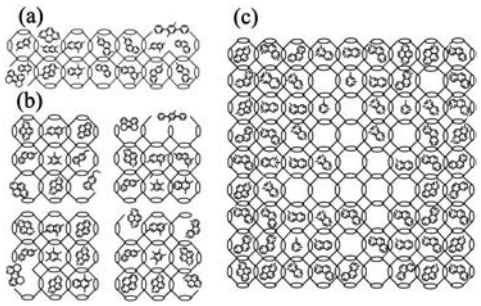

Fig. 7 Coke location and deactivation mode of SAPO-34: (a) SP-S, (b) SP-F, and (c) SP-M and SP-C. Copyright © 2013, American Chemical Society.[52]

2.2 Crystal growth inhibitor-assisted synthesis

In general, the preference for crystal nucleation over crystal growth facilitates the formation of nanocrystals. It has been well demonstrated that the crystal growth inhibitor (CGI) is beneficial for the production of nanocrystals through its strong interaction with the nuclei. On one hand, the CGI interacts with reactive sites of the inorganic species in the synthesis medium, promotes nucleation and results in a large amount of smaller nuclei. On the other hand, the CGI adsorbs onto the surface of nuclei and separate nuclei owing to steric hindrance, which inhibits crystal growth.[40]

Carreon and co-workers synthesized submicrometer-sized SAPO-34 crystals with polyethylene glycol-600 (PEG), polyoxyethylene lauryl ether (Brij-35), and methylene blue (MB) as CGIs. The SAPO-34 crystals exhibited a plate-like morphology of 0.8 × 0.25 μm, 0.7 × 0.2 μm and 0.9 × 0.2 μm, when PEG, Brij-35 and MB were adopted.[59] It is speculated that the CGI adsorbs on the surface of the nuclei due to its larger kinetic diameter than the pore size of SAPO-34, and growth of the precursors is inhibited by the CGI. Furthermore, the introduction of the CGI enhances the alkalinity of the synthesis gel, which promotes the nucleation rate and facilitates the

formation of smaller crystals. Similarly, Shi synthesized SAPO-34 (400–500 nm) with β-cyclodextrin (β-CD) as a CGI under microwave irradiation.[60] It is speculated that β-CD interacts with the reactive sites of the crystal nuclei and facilitates nucleation. Owing to β-CD's coordination and steric hindrance, the nuclei are separated and their growth is inhibited. It is widely acknowledged that the utilization of easily dissolvable silica sources facilitates nucleation and results in the formation of SAPO-34 with small crystal size.[34,61] Lu *et al.* synthesized SAPO-34 crystals of 0.8–1.6 μm with metakaolin, an economical mineral with a low dispersion degree, as silicon and aluminum sources and β-CD as the CGI.[62] The introduction of β-CD reduces the Si-enrichment on the surface, and decreases the acid site density on the surface, which inhibits coke formation in the cages near the surface and ultimately enhances the catalyst stability in the MTO reaction.

2.3 Post-synthesis treatment

The nanosized molecular sieves can also be obtained through post-synthesis treatment which involves milling of the micrometer-sized primary molecular sieves, followed by recrystallization.[63] Liu and co-workers prepared SAPO-34 nanocrystals with a cubic-like morphology (50–350 nm) through a milling and recrystallization method.[64] The crystallinity of the milled micrometer-sized SAPO-34 was recovered by recrystallization in diluted aluminosilicate solution or the recycled mother liquid with TEA as the template. The SAPO-34 nanocrystals exhibit high mesopore volume due to the intercrystal pores of the nanoparticles. After milling and recrystallization, the Si contents on the external surface decrease, resulting in reduced acid strength and amount. Owing to the better utilization of the internal pore space and the reduced acidity, the SAPO-34 nanocrystals exhibit prolonged catalyst lifetime, enhanced selectivity to light olefins and retarded propane production from propylene hydrogenation.

2.4 Dry gel conversion

The dry gel conversion method (DGC) has aroused increasing interest due to the markedly shorter crystallization time compared with the conventional hydrothermal crystallization. The DGC can be categorized into two techniques, steam-assisted conversion (SAC) and vapor-phase transport (VPT). In the SAC technique, molecular sieves are obtained *via* crystallization of a dry gel containing an organic template under water-steaming treatment. In the VPT technique, a dry gel is crystallized at a certain temperature in a steam flow of SDA plus water.

Nishiyama *et al.* synthesized SAPO-34 nanoparticles with an average crystal size of 75 nm through DGC with TEAOH.[65] Owing to the loss of moisture, it is proposed that drying the precursor gel before crystallization induces high nucleation density in the early stages and slow rates of crystal growth after nucleation, which results in the formation of small crystals. Similarly, Halladj *et al.* prepared SAPO-34 with average particle sizes of 300 nm through economical morpholine.[66] The influence of factors such as crystallization time, gel drying temperature and water content on the crystallinity, morphology and particle size of SAPO-34 was thoroughly investigated.

2.5 Ultrasound-assisted synthesis

Recently, sonochemical synthesis by ultrasonic irradiation (20 kHz–10 MHz) based on acoustic cavitation phenomena, the formation, growth and collapse of bubbles in liquid medium, has gained ever-growing research interest. On one hand, the collapse of bubbles generates localized hot spots and provides high temperature (5000–25 000 K) and pressure (181.8 MPa), which break the chemical bonds and accelerate the reactions. On the other hand, the collapse of bubbles occurring in less than a nanosecond yields a high rate of temperature decrease (10^{11} K s^{-1}), which inhibits the further growth and agglomeration of particles.[67]

Halladj and co-workers prepared uniform SAPO-34 nanoparticles of about 50 nm through sonochemical-assisted hydrothermal synthesis (at 200 °C within a short time of 1.5 h).[68] It is proposed that the collapse of a large number of cavitation bubbles supplies high energy, induces the formation of crystal nuclei, promotes nucleation in the early stages and shortens the induction time. Then, the rapid local cooling rates occur after the collapse of bubbles, which decreases the rate of crystal growth after nucleation. Moreover, the impacts of ultrasonic power intensity, sonication temperature, irradiation time and sonotrode size on the physicochemical properties and relative catalytic performance were thoroughly investigated.[69] It is found that the increases of US power, sonication duration and temperature result in SAPO-34 with reduced agglomeration, higher crystallinity and smaller crystal size, owing to the increased number of nuclei and faster nucleation rate.

2.6 Fast high-temperature synthesis

In general, the hydrothermal synthesis of SAPO-34 in a batch-type autoclave in the range of 180–200 °C requires quite a long crystallization time of 24–72 h, which is of high energy consumption and synthetic cost. Though novel synthesis strategies such as microwave-assisted synthesis and dry gel conversion, as well as ultrasound-assisted synthesis, have been provided in recent years, the crystallization time of SAPO-34 still requires about several hours.

Kazemian *et al.* synthesized SAPO-34 crystals through a rapid high-temperature method (400 °C) with a short time of 45 min.[70] The SAPO-34 crystals with an average size of 500–800 nm show the morphology of aggregated nano-sized cubic crystals with a size of 50–200 nm. It is proposed that the high temperature facilitates the rate of nucleation and decreases the rate of crystal growth, resulting in decreased particle size. Nevertheless, emphasis should be laid on the precise control of synthesis time since the high pressure in the high-temperature environment might deteriorate the SAPO-34

structure to some extent. Similarly, Halladj and coworkers synthesized submicron-sized SAPO-34 with a particle size of 491–938 nm through a dry gel method at high temperatures (400 °C) within a short time of 30 min.[71] Nevertheless, the SAPO-34 crystals suffer from decreased crystallinity and low BET surface area.

Recently, Yu and co-workers obtained nano-sized SAPO-34 crystals with high crystallinity in 10 minutes by combining fast oil-bath heating (at 200 °C) in a stainless steel tubular reactor with a seed-assisted method.[72] The nano-sized SAPO-34 crystals exhibit a nanosheet-like morphology with an average size of ~200 × 200 nm. The rapid heat transfer increases the temperature of the initial gel, and the combination of fast heating and seeding accelerates the crystallization rate of SAPO-34 crystals, thus the product yield can reach 80% in 60 minutes. Furthermore, the fast synthesis decreases the incorporated Si content, inhibits the formation of silicon islands and subsequently reduces the acidity. Due to the decreased acidity and enhanced mass transfer of reactants and products, nano-sized SAPO-34 exhibits remarkable performance in the MTO reaction.

2.7 Mixed template synthesis

TEAOH is generally adopted as a template to synthesize nano-sized SAPO-34.[73] However, the relatively high price of TEAOH hampers its large-scale practical application. Therefore, the substitution of sole template TEAOH with mixed templates such as TEAOH/morpholine (Mor),[74,75] TEAOH/triethylamine (TEA),[76] TEAOH/diethylamine (DEA),[77–79] and TEAOH/dipropylamine (DPA)[77,80] opens a new horizon for the preparation of molecular sieves and brings great potential for future industrialization.

Jun *et al.* synthesized submicron-sized SAPO-34 with a mixture of morpholine and TEAOH. The homogeneous spherical SAPO-34 with an average crystal size of 1 μm is composed of aggregates of nano-sized crystals. The crystals obtained with the mixture of 75% morpholine and 25% TEAOH have the longest catalyst lifetime, which may be attributed to the optimum crystal size.[74] Halladj *et al.* investigated the impact of mixtures of two, three and four templates (TEAOH, morpholine, DEA and TEA) on the morphology of SAPO-34. It is found that SAPO-34 obtained with the combination of 75% TEAOH and 25% Mor shows spherical aggregates (400–600 nm) of nanometer-sized particles (100–200 nm) with narrow distribution, while samples obtained by mixing four templates show spherical aggregates (around 500 to 800 nm) of nanosized and homogeneous cubic particles (around 100–200 nm).[81]

3. Synthesis of hierarchical SAPO-34

3.1 "Top-down" approach

3.1.1 Fluoride etching. On one hand, the hydrothermal stabilities of molecular sieve nanocrystals are not always comparable with those of their micrometer-sized counterparts. On the other hand, owing to the high synthetic cost, complicated synthesis process, and difficult separation of the nanocrystals from the colloidal mother liquor by filtration, large-scale industrial application of these nanocrystals is hampered. Additionally, in contrast to the intracrystalline mesopores, the relatively unstable intercrystalline mesopores originating from the self-assembly of nanocrystals are often easily lost, since the treatment stresses during catalytic applications often lead to the tight agglomeration of the nanocrystals.[27,82]

In contrast to the complicated bottom-up approach, the top-down approach is much more simple, economical and scalable. However, on one hand, the acidic or basic post-treatment preferentially extracts the framework Al or Si cations, respectively, which might result into the destruction of Brønsted acid sites in the case of SAPO-type molecular sieves. On the other hand, the alternations of the framework cations make the frameworks of SAPO-type materials not as stable as those of aluminosilicates, thus causing them to be more vulnerable to chemical post-treatment and suffer from the loss of crystallinity after the conventional acidic/alkaline treatment.[83] In a word, the traditional top-down approach, mainly applied for enhancing the catalytic performance of aluminosilicate zeolites, can only be applied to SAPO molecular sieves under precisely controlled conditions.

Valtchev and co-workers demonstrated that bifluoride ions (HF_2) produced from the HF–NH_4F solution indiscriminately extract Si and Al from the zeolite framework.[84] Chen *et al.* developed controlled post-synthesis fluoride etching for the preparation of hierarchically porous SAPO-34 crystals.[85] The secondary pores in the hierarchical SAPO-34 are introduced by treatment in the HF–NH_4F solution under ultrasonic (US) irradiation. The external BET surface areas and the mesopore volumes increase, as a consequence of incorporated secondary porosity. The numbers of Brønsted acid sites of the hierarchical SAPO-34 decrease substantially, which is ascribed to the dissolution of the silicon-rich interfaces between crystalline domains. The intersecting mesopores between the crystalline domains penetrate deeply into the bulk of the crystals, separating the crystals into smaller particles, thus enhancing their access to the micropore space. Therefore, the hierarchical SAPO-34 exhibits longer catalyst lifetime and higher productivity.

Furthermore, Chen *et al.* investigated the influences of organic templates (Mor, TEA and TEAOH) on the fluoride etching process and the related catalytic performance.[86] It is shown that the HF–NH_4F solution is more Si-selective, particularly for SAPO-34–TEAOH, and decreases the Si content and subsequently the strength and concentration of strong acid sites, which is beneficial for the formation of propylene and unfavourable for ethylene production. Thus, the improved selectivity to light olefins over the hierarchical SAPO-34 is attributed to the exposed active sites and the enhanced mass transfer. For the hierarchical SAPO-34–TEA, the ameliorated diffusion, appropriate acidity and retained microporous volume also result in a longer catalyst lifespan. As for the hierarchical SAPO-34–Mor and hierarchical SAPO-34–TEAOH, the decreased crystallinity and decreased acidity lead to a

diminished lifespan. However, the fluoride post-treatment route suffers from relatively high weight loss attributed to the dissolution of crystalline domains (30–45 wt% yield, depending on factors such as organic templates or etching time).

3.1.2 Basic/acidic etching. SAPO-type molecular sieves suffer from amorphization when inorganic base NaOH is employed, thus relatively expensive organic bases should be adopted to preserve the crystallinity.[83,87] Furthermore, the adoption of organic bases as etching agents simplifies the post-treatment steps and avoids the additional ion-exchange process to obtain the protonic form of molecular sieves when inorganic bases are used. In addition, the demetallation process under alkaline post-etching with organic bases is milder and more controllable.[63,88]

Qiao *et al.* synthesized hollow SAPO-34 crystals with a shell thickness of 30–50 nm through selective etching under controlled alkaline (organic amines TEAOH, TPAOH, TMAOH and DEA) or acid (HCL) treatment.[87] The hollow SAPO-34 crystals show increased external surface areas and pore volumes owing to the creation of large voids in the interior of SAPO-34. It is shown that framework P atoms are preferentially extracted in base leaching while framework Al atoms are more susceptible to extraction in acid treatment (Fig. 8). Since more Si–O–Al domains and Si islands are located at the outer layer of the crystals due to the Si-rich external surface, it is proposed that framework Al atoms in the Si–O–Al domains offer strong protection for the Si atoms in the Si–O–Al environment while Si atoms in the Si islands also show better stability than framework P atoms during alkaline treatment. The Si–O–Si networks $(Si(OAl)_n(OSi)_{(4-n)}$, $n = 0–2)$ owing to the Si islands preserve the outer layer from dissolution during the acidic treatment. Nevertheless, the recovery rate of SAPO-34 is not satisfying (25–42%) after the post-treatment. Likewise, Liu and coworkers prepared hierarchically porous SAPO-34 crystals with micro-, meso- and macro-pores through TEAOH.[89] The SAPO-34 crystals exhibit scattered pores on the top and bottom surfaces and an hourglass-like, symmetric, touching triangle pore pattern on the other four side surfaces. It is proposed that the desilication process with Al and P homogeneously etched off at the same time introduces additional meso- and macro-pore structures and well preserves the acidity of the parent SAPO-34. The hierarchical SAPO-34 shows longer single-run lifetime and higher stability during the harsh reactivation cycling due to the improved mass transfer.

Taking the high price of organic amines such as TEAOH into consideration, Liu and coworkers further prepared hierarchical SAPO-34 with micropores, mesopores (40–50 nm) and macropores (62–500 nm) through post-etching with nitric acid and oxalic acid.[90] The hierarchical SAPO-34 presents butterfly-shaped porous patterns on four side faces. Due to the synergistic effect of the hierarchical pores and slightly decreased strong acid sites, the hierarchical SAPO-34 shows a lower coking rate, increased coke capacity and prolonged catalyst lifetime. The recovery rate of the acid-treated samples (70% and 72% for nitric acid and oxalic acid, respectively) was higher compared to those post-etched with organic amines, nevertheless, the acid-etched samples suffer from decreased crystallinity (25% and 27% for nitric acid and oxalic acid, respectively) owing to the generated defects in the framework. It is proposed that the crystal skeleton consists of eight pyramidal sub-crystals at first, then the filling of voids in the center part of the crystal leads to their growth into a cubic crystal. Also, the acidic or basic post-treatment preferentially etches the subsequently formed parts of SAPO-34 probably owing to the shorter crystallization time and poorer stability.[91]

3.2 "Bottom-up" approach

3.2.1 Hard template. In general, the "top-down" approach suffers from relatively high weight loss (depends on the etching agents), attributed to the dissolution of crystalline domains.[85] In addition, the size, shape, and number of mesopores are not controllable, and the harsh dissolution conditions may induce the formation of crystal defects. Finally, the "top-down" approach usually requires the time-consuming and waste-producing washing process.

For the first time, Kaskel *et al.* synthesized hierarchical SAPO-34 through adopting carbon materials (nanotubes and nanoparticles) as hard templates (Fig. 9).[92] The generated cave-like mesopores in samples templated with carbon nanoparticles are located inside the particles and inaccessible to

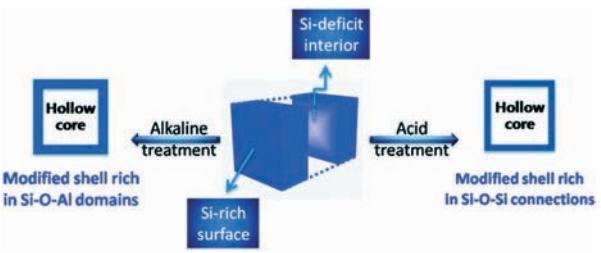

Fig. 8 Formation mechanisms of hollow SAPO-34 by acidic and alkaline treatments. Reproduced from ref. 87 with permission from The Royal Society of Chemistry.

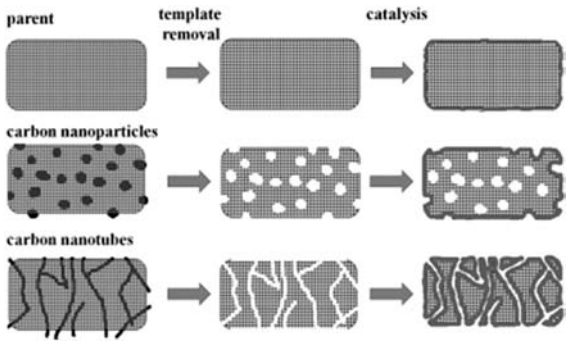

Fig. 9 Synthesis route and catalytic efficiency. Copyright © 2012, Elsevier.[92]

the external surfaces of the crystals, thus no obvious improvement in the catalytic performance is observed. In contrast, hierarchical SAPO-34 templated using carbon nanotubes (CNT) exhibits longer catalyst lifetime and higher product selectivity.

Likewise, Jhung *et al.* developed hierarchical SAPO-34 with carbon black as the hard template under microwave irradiation.[93] The enhanced catalytic stability and catalyst lifespan for the dehydration of butanol and ethanol were ascribed to the increased secondary mesoporosity. The mesopore volume and the pore size can be modified by the amount of carbon black and the particle size of carbon black. Similarly, Halladj *et al.* synthesized hierarchical SAPO-34 by a dry gel conversion method with CNT as the hard template.[94] The introduced mesoporous structure is believed to be able to enhance the mass transfer and prevent undesirable side reactions.

3.2.2 Soft template

3.2.2.1 Polymer. Hard templates such as carbon materials are usually hydrophobic, which leads to the weak interaction between the synthesis gels and the hard templates.[32] In addition, the hard-template approach is relatively costly and commonly requires the unavoidable post-treatment to remove the solid template after crystallization, which hampers its further industrial application.[15] In contrast to hard templates, soft templates yield hierarchical molecular sieves with well-controlled mesopores in a facile one-step manner. Due to their three-dimensional networks, abundant functional groups and designed molecular sizes, a wealth of polymers have been demonstrated to be excellent mesoporous templates by forming a polymer network inside the molecular sieve matrix, and exert great impacts on crystal nucleation and growth.[95,96] For instance, polyethylene glycol (PEG), a highly flexible water-soluble linear polymer with low toxicity, has been widely applied in the incorporation of secondary mesopores in SAPO-34.

Wei and co-workers obtained hierarchically porous crisscross-like SAPO-34 agglomerated from nanocrystals with PEG as the mesoporogen.[97] The hierarchical SAPO-34 exhibits enhanced selectivity to propylene and high stability in the conversion of dimethyl ether (DME) to olefins (DTO), which is attributed to the enhanced intracrystalline diffusion and retarded secondary reaction. It is speculated that PEG micelles interact with the synthesized gel through hydrogen bonding of the ethylene oxide groups, which are embedded into the crystals, and induce the formation of mesopores. However, an excess amount of PEG results in an increased particle size, which is disadvantageous for the diffusion of the DME feedstock. Likewise, Fatemi *et al.* synthesised hierarchical SAPO-34 with a mesopore diameter of about 9 nm employing PEG as the mesopore-generating agent and crystal growth inhibitor *via* a self-assembly strategy.[98] In addition to the role of induction of mesopores, owing to the function of swelling and water content reduction, PEG leads to a high degree of supersaturation and accelerates the nucleation rate.[59] Moreover, it is speculated that PEG chains occupy the surface of the nuclei, increase the electrostatic repulsion force between individual crystals and retard crystal aggregation, which favour the formation of more uniform and smaller crystals. Wang *et al.* synthesized nanoplate-like SAPO-34 with PEG as the porogen.[99] The nanoplates exhibit uniform size (200–400 nm) with a thickness of 40–50 nm. The nanoplate-like SAPO-34 provides large external surface areas and short diffusion length, and the intra-crystalline mesoporous structures with a size of about 2–10 nm further facilitate mass transfer, resulting in excellent catalytic performance in the dehydration of fructose into 5-hydroxymethylfurfural.

In addition, Yu and co-workers prepared hierarchical SAPO-34 with intracrystalline micro–meso–macroporosity through an Al-rich method and PEG 2000.[100] The hierarchically porous SAPO-34 crystals show a center-hollowed morphology with micrometer-sized macroholes (*ca.* 2 mm) in the central crystal and nanometer-sized macrochannels (*ca.* 100 nm) on the surfaces and extending along the entire crystal network. The hierarchically porous SAPO-34 crystals exhibit about six times prolonged catalytic lifespan, which can be ascribed to the enhanced mass transfer of the products from the narrow pore to outside space. Moreover, the hierarchical pores offer more space to accommodate larger coke species such as phenanthrenes and pyrenes, while smaller coke species such as benzenes and naphthalenes easily escape out of the crystals, thus the formation into larger organic species is inhibited, which is also beneficial for the prolongation of the catalyst lifespan. The trilevel hierarchical SAPO-34 exhibits higher selectivity to ethylene and propylene, which can be attributed to the decreased strength and concentration of strong acid sites. The PEG micelles are embedded into the molecular sieve matrix through attracting the precursors onto the surface of PEG micelles, and direct the formation of mesoporous structures (Fig. 10). Meanwhile, the superfluous aluminium in the SAPO-34 framework produces more terminal groups and defects, leading to the formation of nanometer-sized macropores. The preferentially etched central parts of the crystal result in the formation of a hollow morphology with micrometer-sized macroholes.

Similarly, polyethyleneimine (PEI), a dendrimer with a repeating unit composed of an amine group and a two-carbon

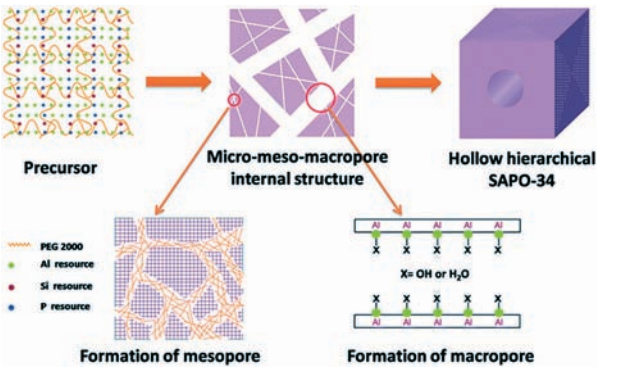

Fig. 10 The process forming the hollow SAPO-34 with the tri-level hierarchically intracrystalline micro–meso–macro-pore structure. Reproduced from ref. 100 with permission from The Royal Society of Chemistry.[100]

chain, was also exploited as a porogen. Jiang *et al.* synthesized hierarchical SAPO-34 with protonated, non-silylated PEI for the formation of intracrystal mesopores.[101] The mesopore volume and mesoporous pore size are tuneable through the molecular weight and the amount of PEI. Moreover, under acidic conditions, the elongated protonated PEI chains interact with oxide species in the sol–gel system through non-covalent bonds such as hydrogen bonding and van der Waals forces, and interconnected continuous mesopores along the main linear chains of PEI are formed after calcination. In contrast, under basic conditions, the coiled PEI minimizes the interaction between PEI aggregates and zeolite precursor molecules, which is not beneficial for the encapsulation of PEI aggregates in the zeolite matrix.

Zhu *et al.* prepared hierarchical nanosized SAPO-34 through hindering the aggregation of primary nanocrystallites with 1,2,3-hexanetriol as a crystal growth inhibitor.[102] The uniform nanosized SAPO-34 (50–100 nm) particles are composed of intergrown cubic primary crystallites (20–50 nm). The hierarchical SAPO-34 crystals exhibit both intracrystal mesopores attributed to void space inside the crystals during oriented attachment and intercrystal mesopores resulting from packing of nanosized crystallites, as demonstrated by TEM images of a Pt replica. It is proposed that dry gel conversion of SAPO-34 follows the oriented attachment (OA) growth mechanism, *i.e.*, aggregative growth mechanism.[103–105] The firstly formed lamellar precursors undergo phase transformation to discrete SAPO-34 nanocrystallites. Owing to the high supersaturation, the nucleation rate is enhanced and the nucleation time is shortened, leading to the formation of great amounts of uniform primary crystallites. Then, the primary nanocrystallites grow into bulky crystals *via* oriented mutual attachment as a result of grain boundary elimination. Therefore, through the strong interaction with crystal surfaces, hierarchical nanosized SAPO-34 can be obtained with 1,2,3-hexanetriol through repressing the intergrowth of primary crystallites formed after precrystallization (Fig. 11). The hierarchical nanosized SAPO-34 exhibits prolonged catalytic lifespan in the chloromethane-to-olefin conversion owing to the retained acidity and the enhanced mass transfer.

3.2.2.2 Cationic surfactants. It has been demonstrated that cationic surfactants are of great significance for the incorporation of mesopores for aluminosilicate zeolites. Liu *et al.* introduced mesoporosity to microporous SAPO-34 with cetyltrimethylammonium bromide $N(CH_3)_3C_{16}H_{33}Br$ (CTAB), a conventional cationic surfactant in the synthesis of mesoporous silicas, and sodium dodecyl sulfate (SDS) as mesopore-generating agents.[106] Additionally, both CTAB and SDS result in the reduction in total acidity amount. In the chloromethane-to-olefin reaction, the enhanced selectivity to propylene over the modified SAPO-34 with SDS and CTAB as the additives was ascribed to the reduction in total acidity and the subsequent inhibition of secondary reactions. Likewise, the longer catalyst lifespan stemmed from the enhancement in diffusivity and the optimal acidity in the SAPO-34. Nevertheless, it is noteworthy to highlight that CTAB often failed to function as a mesopore-directing agent when the surfactant was added to the synthetic mixtures with the aim to synthesize hierarchical molecular sieves, and phase separation of crystalline microporous molecular sieves and amorphous mesoporous materials was observed.

Different from the pure template function of polymers, organosilane surfactants, acting simultaneously as parts of the silica source and mesoporogens during the synthesis, influence the crystalline growth and the morphology and textural properties of the SAPO molecular sieves, and prevent the phase separation of microporous and mesoporous structures. In particular, amphiphilic quaternary ammonium-type organosilane surfactants composed of a hydrolysable alkoxy moiety, a zeolite structure-directing group of quaternary ammonium, and a hydrophobic alkyl moiety interact with the growing crystal matrix domains and direct the formation of the mesostructure by forming a micelle through the covalent bonds between the methoxysilyl moiety and other silica sources.[107,108]

Ma *et al.* prepared hierarchical SAPO-34 with phenylaminopropyltrimethoxysilane (PHAPTMS) as the mesoporogen and a part of the silicon source and TEAOH as the microporous structure-directing agent.[109] The hierarchical SAPO-34 particles with a crystal size of approximately 1.0 μm are composed of nanocrystals (*ca.* 50 nm). The incorporated hydrophobic moiety in PHAPTMS inhibits the growth of the crystals, leading to the self-assembly of nanocrystals, and the intercrystal mesoporous void results from the aggregation of the nanocrystals. PHAPTMS leads to a higher density of weak acidic sites and a lower density of strong acidic sites, which retard the hydrogen transfer reaction of olefins to saturated hydrocarbons and aromatics. Additionally, the reduced crystal size alleviates the diffusion limitation and subsequently inhibits coke formation.

In 2010, Qiu *et al.* synthesized hierarchical SAPO-34 with [3-(trimethoxysilyl)propyl]octadecyldimethylammonium chloride (TPOAC) as the mesopore-generating agent and sole silica source and TEAOH as the microporous template.[110] The hierarchical SAPO-34 exhibits much weaker acidity than conventional SAPO-34, and its application in the MTO reaction has not been investigated. Ahn *et al.* prepared hierarchical SAPO-34 with reduced crystal size using TPOAC under microwave conditions.[111] The improved reactivity and especially

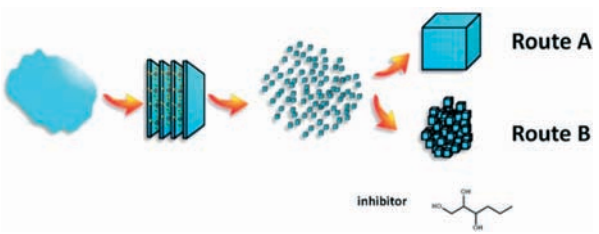

Fig. 11 Proposed formation mechanism of SAPO-34 through the oriented attachment mechanism (A) and the synthetic strategy for hierarchical SAPO-34 (B). Copyright © 2015 Elsevier Inc. All rights reserved.

slower catalytic deactivation rates in the MTO reaction were attributed to the optimal acidity, the presence of mesoporosity, particle size reduction and the consequently reduced diffusion path. Similarly, Hensen and co-workers synthesized mesoporous SAPO-34 with the mesoporogen TPOAC.[112] Meanwhile, they noted that $(C_{22}H_{45}–N^+(CH_3)_2–C_4H_8–N^+(CH_3)_2–C_4H_9)Br_2$ ($C_{22\text{-}4\text{-}4}Br_2$) was unable to introduce secondary mesoporosity. However, the additional intracrystalline mesoporosity has no positive influence in enhancing the catalytic stability and lowering the deactivation rate, since the mesoporous SAPO-34 contains a lower concentration of Brønsted acid sites. The total methanol conversion capacity per Brønsted acid site of the mesoporous SAPO-34 is comparable to that of the original microporous SAPO-34, which is attributed to the efficient utilization of the micropores of SAPO-34 in the MTO reaction. Taghizadeh *et al.* found that the nanosized hierarchical porous SAPO-34 templated with a mixture of 50% TPOAC and 50% CTAB exhibits an improved catalyst lifespan along with enhanced selectivity to light olefins, which is originated from the optimized acidity and the additional mesoporosity.[113]

Quite recently, Yu and co-workers successfully synthesized hierarchical porous SAPO-34 using TPOAC as the mesopore director and Mor as the microporous template by one-step hydrothermal crystallization.[114] The cubic-shaped micrometer-sized SAPO-34 results from the agglomeration of cubic-like nanocrystals, which exhibit a remarkably prolonged catalyst lifespan and excellent light olefin selectivity in the MTO reaction. Firstly, the hierarchical SAPO-34 exhibits lower acidic strength and acidic concentration of strong acid sites, which inhibit coke formation. In addition, the incorporated mesopores enhance the transfer of the products from the narrow pore to outside space. Similarly, the small nanocrystals shorten the diffusion length of reactants and products, thus greatly enhancing the mass transfer. Last but not least, the hydrophobic alkyl tails of TPOAC attached on the surface of nanocrystals through the capping effect,[115] thus inhibiting the nanocrystals from further growth and leading to the assembly of the nanocrystals with large mesopores between the nanocrystalline domains (Fig. 12).

Similarly, Liu and co-workers synthesized hierarchical SAPO-34 with TPOAC as the mesoporogen and a part of the silica source and DEA as the microporous template.[116] The impact of the microporous template on the synthesis of hierarchical SAPO-34 was thoroughly investigated. It is observed that the introduction of TPOAC decreases the acidity of SAPO-34, thus DEA, the microporous template that is able to introduce more silica into the framework and results in more acidic sites, was adopted. The morphology evolves from spherical agglomerates consisting of micrometer-sized cubic crystals, to self-assemblies of spherical nanosheets spliced by nano-square pieces, and then aggregates of *ca.* 50 nm particles with the increase of the TPOAC/TEOS ratio. It is proposed that the SAPO precursors adsorbed with surfactants evolve to rhombohedral crystals when a small amount of TPOAC is employed, and the self-assembly of TPOAC directs the formation of intergrown SAPO-34 nanosheets when a suitable concentration of TPOAC is adopted, but only nanoparticles are formed when a high amount of TPOAC is involved, which results from the inhibition of crystal growth by the surfactants (Fig. 13). Liu and coworkers further synthesized mesoporous SAPO-34 single crystals by combining the milled SAPO-34 precursor with the TPOAC mesoporogen within 4 hours.[117] It is believed that the SAPO-34 precursor accelerates the crystallization rate of the microporous structure, while the TPOAC facilitates the incorporation of mesopores. The connectivity in the porous structures has been well proved by variable-temperature laser-hyperpolarized (HP) ^{129}Xe NMR and 2D-NMR exchange spectroscopy (EXSY). Due to the reduced acidity and enhanced diffusion efficiency, the mesoporous SAPO-34 synthesized through the reconstruction method exhibits an enhanced catalyst lifespan.

Considering the fact that the incorporation of P from an organophosphorus surfactant into the SAPO framework has no impact on the acidity, Liu *et al.* synthesized hierarchical SAPO-34 with [2-(diethoxyphosphono)propyl]-hexadecyldimethylammonium bromide $[(C_2H_5O)_2P(O)–C_3H_6–N(CH_3)_2–C_{16}H_{33}]Br$ (DPHAB).[118] The morphology evolves into spherical aggregates of the crystals with the increased DPHAB/H_3PO_4 ratio in the reactant gel. Similar to the previous reports,[58,119] the enhanced propylene and reduced

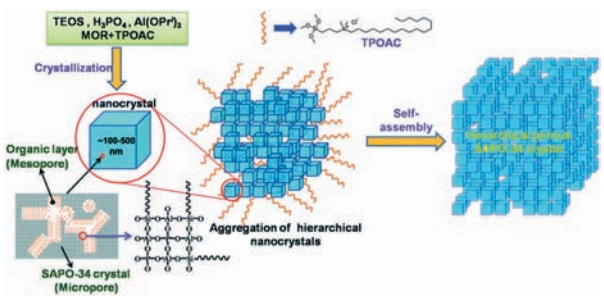

Fig. 12 Assembly pathway of hierarchical SAPO-34 crystals aggregated from cubic nanocrystals assisted by the organosilane surfactant. Reproduced from ref. 114 with permission from The Royal Society of Chemistry.[114]

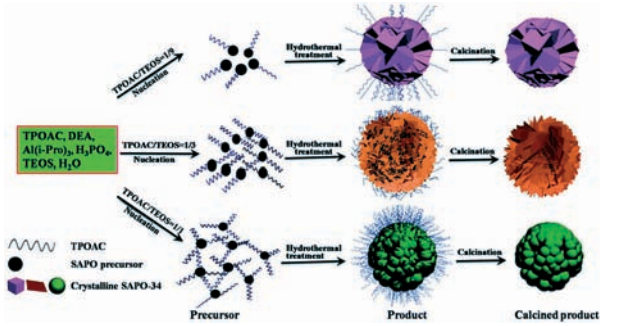

Fig. 13 The proposed crystallization process of SAPO-34s with different TPOAC/TEOS ratios. Reproduced from ref. 116 with permission from The Royal Society of Chemistry.[116]

ethylene selectivity originates from the intercrystal mesopores and subsequently improved mass transfer ability, and the improved catalytic performance is ascribed to the well-maintained acidity. According to the molecular electrostatic potential (MEP), for DPHAB, the quaternary ammonium group exhibits nucleophilic reactivity, indicated by the positive (blue) regions, interacting with the anionic SAPO species through nucleophilic reactions, However, owing to the existence of P═O for DPHAB, the electrophilic reactivity in the vicinity of the diethoxyphosphono groups (the green colour), indicated by the negative (red) region, inhibits the interaction between the DPHAB and SAPO species (Fig. 14). As a result, the quaternary ammonium groups and the long alkyl chains of DPHAB are incorporated in the final product, resulting in a mesoporous structure, while the diethoxyphosphono groups and the hydrolyzed products stay in the mother liquid.

Considering the high cost of amphiphilic quaternary ammonium-type organosilane surfactants, Liu *et al.* further synthesized SAPO-34 nanoaggregates with nonsurfactant organosilane 3-piperazinepropylmethyldimethoxysilane (PZPMS), as a crystal growth inhibitor, a part of the silica source and a co-template.[120] The spherical SAPO-34 aggregates (~1 μm) are composed of cubic nanocrystals (100–200 nm). The propylmethyldimethoxysilane group of PZPMS functions as a part of the silica source and inhibits crystal growth, while the piperazinyl group of PZPMS, as a co-template, suppresses SAPO-34/18 intergrowth. The SAPO-34 nanoaggregates exhibit a prolonged lifespan and lower coking rate, which is ascribed to the reduced crystal size and lower acid concentration, and the facilitated diffusion and mass transportation in the MTO reaction.

3.3 Other approaches

3.3.1 Hollow SAPO-34. Hollow zeolites and zeotype materials, as a class of materials in which diffusion limitations can be reduced by the small thickness of microporous walls, have recently received rapidly growing attention.[121] In general, zeolites and zeotype materials prepared in fluoride medium show better crystallinity and fewer defects.[122,123] Zhang *et al.* prepared floral mesoporous SAPO-34 with NaF addition by a hydrothermal method, which is attributed to the eroding effect of fluoride ions.[124] Very recently, Yu and coworkers prepared hierarchically macroporous SAPO-34 through a one-step HF-assisted *in situ* growth-etching route.[91] HF serves as not only a mineralizer but also a chemical etching agent. HF indiscriminately extracts both framework Si and Al(P), and does not decrease the crystallinity since etching occurs during crystallization. The SAPO-34 contains micrometer-sized macroholes in the central part and intracrystalline nanometer-sized macrochannels. The hierarchically macroporous SAPO-34 exhibits relatively strong acidic strength and decreased external surface acidity due to the decreased Si content on the external surface. The increased acidic strength lowers the energy barrier for ethylene production, while the reduction of the external acid sites inhibits the less-selective reaction occurring on the external acid sites, which leads to the enhanced selectivity to ethylene. At the early stage of crystallization, a crystal morphology consisting of eight pyramidal parts is observed. The voids in the vicinity of the center are then filled up by crystal growth until regular rhombohedral crystals are obtained. The macroholes in the central part originate from the secondary dissolution by HF in mother liquids, and the macrochannels result from the preferential etching of HF at small intergrowth domains, while the holes on the crystal surface results from the dissolution of defect regions (Fig. 15). The hierarchically macroporous SAPO-34 facilitates the diffusion of smaller coke species such as benzene and naphthalene and contains macroporous spaces to accommodate larger coke species such as phenanthrene and pyrene, thus inhibiting catalyst deactivation. Moreover, the formation of macropores provides more external active sites, which enhance the catalyst activity.

Zhang and co-workers developed a novel biomineralization preparation method and synthesized hollow SAPO-34 cubes by a vapor-phase transport (VPT) method from gelatin-containing solid precursor gels.[125] A reversed crystal growth process, namely, surface-to-core crystal growth route, was proposed. The hollow SAPO-34 cubes were composed of symmetrically arranged four two-top-point truncated octahedra with layered square-like nanoplates encapsulated by dense

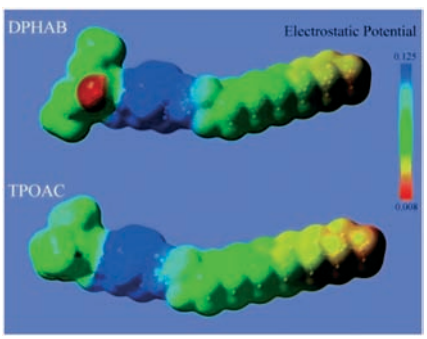

Fig. 14 Molecular electrostatic potential maps of DPHAB and TPOAC. Reproduced from ref. 118 with permission from The Royal Society of Chemistry.[118]

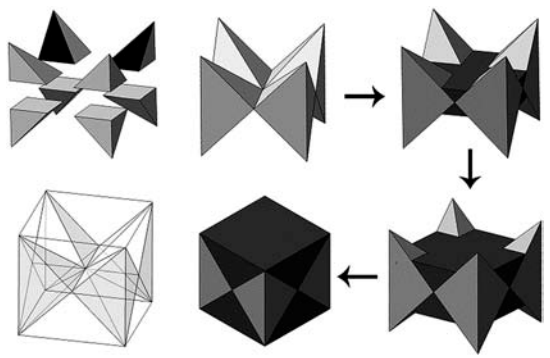

Fig. 15 Schematic representation of the proposed evolution process of the hierarchically macroporous SAPO-34. Reproduced from ref. 91 with permission from The Royal Society of Chemistry.[91]

crystalline shells. Hollow SAPO-34 cubes cut by a focused ion beam (FIB) miller show an X-shaped hollow in the middle, constructed from two isosceles triangle-shaped solid parts. At the early stage, amorphous aggregates with a layered structure owing to the interaction of gelatin and aluminophosphate precursor species were formed and confined inside the rectangular boxes. The hollow structure with four two-top-point truncated octahedra was formed by consuming the internal amorphous aggregates (Fig. 16).

Wang *et al.* synthesized hierarchical SAPO-34/18 with an intergrowth structure (CHA and AEI structure ratio of 8 : 2) through decreasing the Si content.[126] The hierarchical SAPO-34/18 was composed of four pyramids and two frustums, with the macropores at the crisscross intersection of the four pyramids forming a well-ordered channel network. The presence of macropores results in shorter mass transfer path lengths and much less intracrystalline diffusion resistance. With the benefit of the hierarchical structure and lower acidity, a longer catalyst lifetime, slower coke deposition rate, and lower selectivity to propane were obtained.

3.3.2 Mother-liquor-reuse synthesis. In general, the synthesis of molecular sieves requires excess amounts of reactants. After the desired products are filtered from the reaction mixture, the filtrate (mother-liquor) containing abundant nutrients, particularly organic species (usually toxic and expensive), is discarded as a waste solution, which increases the synthesis cost and leads to environmental pollution.[127] Yu and coworkers synthesized hierarchical SAPO-34 through recycling of waste mother-liquors containing HF (Fig. 17).[128] The hierarchical SAPO-34 exhibits a center-hollowed morphology with intracrystalline macropores originated from the dissolution of defect regions. The hierarchical SAPO-34 synthesized through recycling mother-liquors shows prolonged catalyst lifetime due to the enhanced diffusion within the macrochannels. Furthermore, samples synthesized through mother-liquors after three recycles still show similar catalytic activities.

3.3.3 Solvothermal or solventless synthesis. Recently, 2-dimensional (2D) zeolites, consisting of extended sheets with thickness limited to 2–3 nm, the dimension corresponding to 1–2 crystallographic unit cells, have received extensive

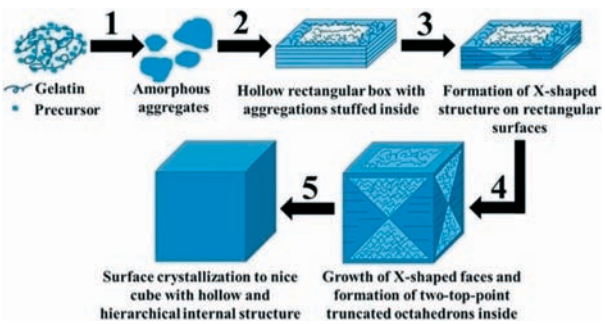

Fig. 16 Schematic drawing of a proposed crystal growth route towards hollow SAPO-34 cubes with a hierarchical internal structure. Copyright © 2014, American Chemical Society.[125]

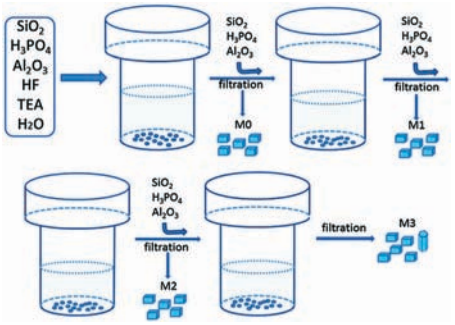

Fig. 17 The illustration of the mother-liquor recyclable synthesis of SAPO-34. Reproduced from ref. 128 with permission from The Royal Society of Chemistry.[128]

attention. Due to the large number of active sites on the external surface, easy accessibility of Brønsted sites, short diffusion distance and fast mass flow, 2D zeolites show high practical potential in adsorption and catalysis.[129] Zhang and colleagues developed a biosynthesis route to prepare hierarchical SAPO-34 with rapeseed pollen extract as the synthesis solution. The hierarchical SAPO-34 shows a spherical blooming flower-like structure composed of a great amount of curly nano-sheets and void space between nano-sheets. Owing to the nano-sheet-constructed structure, the hierarchical SAPO-34 exhibits higher diffusion rates, a high CO_2 adsorption capacity and high CO_2/CH_4 separation factors in gas separation.[130]

Owing to the associated undesired issues of hydrothermal or solvothermal synthesis, including environmental pollution, high autogenous pressure and the consequent equipment safety factor, low utilization efficiency of the autoclaves, reduced yield of zeolite products and high energy consumption,[127,131] solvent-free synthesis strategies, satisfying the standard of *E*-factor and the principles of green chemistry,[132] have attracted extensive research interest. Considering the fact that water serves as a reactant to hydrolyse the silica source to form active silica species with attached OH groups at the beginning of the crystallization process and as a by-product during the crystallization process owing to the condensation of active silica species into zeolite products,[133] Xiao and colleagues prepared hierarchical SAPO-34 through a novel solvent-free synthesis method by mechanical mixing, grinding, and heating of the raw materials $NH_4H_2PO_4$, boehmite, fumed silica, and Mor.[119] The hierarchical SAPO-34 consists of micro-, meso-, and macropores, and the presence of meso- and macrostructures might originate from the existence of voids between the starting materials and the unique crystallization process in a solvent-free manner. SAPO-34 shows higher selectivity for propylene and butylene and reduced selectivity for ethylene, due to the unique micro–meso–macroporous structure and the consequently enhanced diffusion.

3.3.4 Seed-assisted synthesis. It is widely accepted that crystal seeds may contain the building units such as secondary building units (SBUs) that play a structure-directing role in crystallization, therefore, the introduction of crystal seeds

into the starting gels is favourable for nucleation and effectively accelerates the crystallization rate.[72,127]

Yu and co-workers synthesized nano-sized hierarchical SAPO-34 through the seed-assisted method with the economical TEA as the template.[134] The hierarchical SAPO-34 presents reduced crystal sizes (300–800 nm) and exhibits a centre-hollowed morphology with intracrystalline meso–macroporosity (25–300 nm) and intercrystalline macropores (800 nm). It is proposed that SAPO-34 crystallizes on the surface of nanosheet-like seeds that covered the inside of the initial gel and etched into fragments. The seeds are dissolved into the gel phase, meanwhile, the precursors crystallize and crystals grow continually, introducing more void spaces (Fig. 18). The reduced crystal size and hierarchical structure enhance the diffusion efficiency and inhibit the coke formation rate. In addition, it is shown that nano-sized hierarchical SAPO-34 exhibited reduced strength and concentration of strong acid sites, which suppress the coking rate. Attributed to the advantages of decreased acidity, reduced crystal size and a hierarchical structure, nano-sized hierarchical SAPO-34 zeolites show prolonged catalyst lifetime and improved selectivity to ethylene and propylene reaching up to 85.0% under the conditions of 673 K with WHSV = 2 h^{-1}.

3.3.5 Nanoscale confined environment-assisted synthesis. Wei *et al.* synthesized hierarchically porous SAPO-34 through a non-mesoporous template process using natural layered kaolin.[135] The sphere-like particles are composed of decussate 60 nm slice-like units, with mesopores formed between neighboring slices. Kaolin not only acts as the silicon and aluminum sources, but also influences the crystal growth and morphology through the layered structure. It is proposed that kaolin transformed into metakaolin, during which the alumina octahedra of kaolin became the aluminum source for crystallization, while the silicon–oxygen tetrahedral layers remained the same. The nanoscale confined gallery spaces between two neighboring silica layers influenced the zeolite preferential growth, and zeolite slice growth changed from one orientation to three orientations (Fig. 19). Nevertheless, it is noteworthy that tuning the Si/Al ratio of the product with kaolin as the raw material is difficult. The enhanced conversion was ascribed to the presence of the hierarchical structure that shortened the diffusion path, facilitated intracrystalline diffusion, and increased accessibility to the active sites.

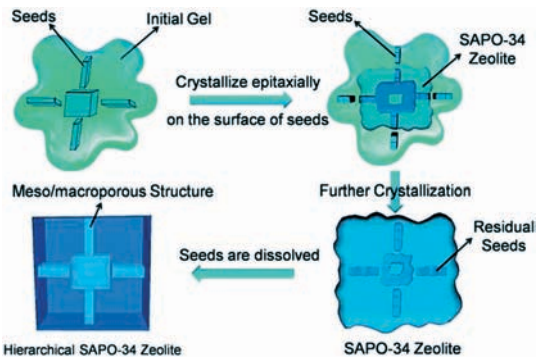

Fig. 18 Schematic of the process for the formation of nano-sized hierarchical SAPO-34. Reproduced from ref. 134 with permission from The Royal Society of Chemistry.[134]

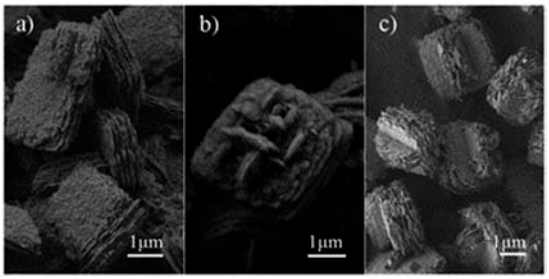

Fig. 19 SEM images of hierarchical SAPO-34 synthesized for (a) 6 h, (b) 10 h and (c) 20 h, showing the preferential growth changing from one orientation to three orientations. Reproduced from ref. 135 with permission from The Royal Society of Chemistry.[135]

3.3.6 Hierarchical SAPO-34 monolith. Xie and coworkers prepared a hierarchically porous SAPO-34 monolith with a micro–meso–macrostructure through the steam-assisted dry gel conversion of an amorphous silicoaluminophosphate monolith.[136] Besides the bicontinuous macropores (6 mm), the small macropores (1 mm) result from the interconnected spherical aggregates of 400–600 nm cubic crystals, while the mesopores arise from the presence of interspaces formed by close stacking of cubic SAPO-34 crystals. The zeolitization of the silicoaluminophosphate gel follows a dissolution–precipitation mechanism including the dissolution of amorphous skeletons, formation of crystal nuclei and growth of crystals. The hierarchical porosity is beneficial for the mass transportation and inhibition of coke formation, which lead to improved catalytic activity in the MTO reaction.

4. Characterization techniques

It must be emphasized that the catalytic activity is strongly affected by the diffusion of reactants and products towards and from the active site, therefore, the efficiency of mesoporosity toward catalytic performance improvement is strongly related to the interconnectivity between micro- and mesopores (sometimes macropores).[137] Currently, for the majority of reports mentioned above, the improved catalytic performance of hierarchical molecular sieves has been ascribed to enhanced mass transfer or the shortened diffusion path without providing persuasive evidence of the diffusion properties. Therefore, in addition to the conventional gas physisorption characterization and mercury intrusion porosimetry,[138,139] other advanced techniques such as confocal fluorescence microscopy, X-ray tomographic microscopy, and NMR-based techniques (*e.g.*, variable-temperature laser-hyperpolarized (HP) ^{129}Xe NMR and 2D-NMR exchange spectroscopy (EXSY))[117,140] should also be explored.[28] In particular, more attention should be focused on three-dimensional electron tomography through 3D reconstruction[141–144] that shed more insights into the

mesoporous structure (connectivity, shape, size, location, accessibility and tortuosity) in hierarchical molecular sieves.

5. Conclusions and outlook

During the last decade, owing to the alleviated diffusion limitations of reactants/products, nanosized and hierarchical SAPO-34 have played a vital role in the methanol-to-olefin conversion processing and other applications (*e.g.*, chloromethane-to-olefin reaction, selective gas adsorption and biomass conversion). This minireview presents a brief overview on the preparation of nanosized SAPO-34 (*e.g.*, microwave-assisted synthesis, crystal growth inhibitor-assisted synthesis, post-synthesis treatment, dry gel conversion, ultrasound-assisted synthesis, fast high-temperature synthesis and multi-template synthesis). The synthesis strategies developed so far for hierarchical SAPO-34 have also been classified and elucidated, including the top-down approach (fluoride etching, basic/acidic etching) and the bottom-up approach (hard templates, soft templates such as polymers and cationic surfactants). Other new approaches such as mother-liquor-reuse synthesis, solvothermal or solventless synthesis, seed-assisted synthesis, nanoscale confined environment-assisted synthesis and hierarchical SAPO-34 monolith have also been illuminated. In addition, emphasis has been put into the current characterization techniques for the mesoporous structure (*e.g.*, pore connectivity) of hierarchical SAPO-34. It is worth noting that the development in the novel, green, facile, and cost-effective synthetic approaches for nanosized/hierarchical molecular sieves will be the main research direction, and the relationship between the mesoporous structure and diffusion properties and the subsequent catalytic performance of the nanosized/hierarchical molecular sieves will also attract extensive interest in the near future. This minireview discussed the advances in fundamental understanding of the rational synthesis of nanosized/hierarchical SAPO-34, with desired properties such as suitable acid strength and amount, decreased diffusion path length, alleviated diffusion limitation, reduced coke formation and prolonged catalyst lifetime. We hope that this review will inspire more novel research to develop the potential and overcome the challenges associated with the synthesis and catalytic applications of nanosized/hierarchical molecular sieves.

Conflicts of interest

There are no conflicts to declare.

Acknowledgements

We thank the National Natural Science Foundation of China (21603223) for financial support.

Notes and references

1 F. Di Renzo and F. Fajula, *Stud. Surf. Sci. Catal.*, 2005, **157**, 1–12.
2 R. Xu, W. Pang, J. Yu, Q. Huo and J. Chen, in *Chemistry of Zeolites and Related Porous Materials: Synthesis and Structure*, 2007, pp. 19–116.
3 C. Baerlocher and L. B. McCusker, *Database of Zeolite Structures*, http://www.iza-structure.org/databases/.
4 C. Baerlocher, L. B. McCusker and D. H. Olson, *Atlas of Zeolite Framework Types*, Amsterdam, 2007.
5 M. Niwa, N. Katada and K. Okumura, *Characterization and Design of Zeolite Catalysts: Solid Acidity, Shape Selectivity and Loading Properties*, Springer, Berlin Heidelberg, 2010, pp. 1–8.
6 M. Guisnet and J. P. Gilson, in *Zeolites for Cleaner Technologies*, Imperial College Press, 2002, vol. 3, pp. 1–28.
7 J. Weitkamp, S. Ernst and L. Puppe, in *Catalysis and Zeolites*, Springer, 1999, pp. 327–376.
8 B. Smit and T. L. M. Maesen, *Nature*, 2008, **451**, 671–678.
9 J. A. Lercher, A. Jentys and A. Brait, in *Acidity and Basicity*, Springer, Berlin Heidelberg, 2008, pp. 153–212.
10 S. Kulprathipanja, *Zeolites in Industrial Separation and Catalysis*, Wiley, 2010.
11 P. Tian, Y. Wei, M. Ye and Z. Liu, *ACS Catal.*, 2015, **5**, 1922–1938.
12 M. Hartmann, A. G. Machoke and W. Schwieger, *Chem. Soc. Rev.*, 2016, **45**, 3313–3330.
13 K. Li, J. Valla and J. Garcia-Martinez, *ChemCatChem*, 2014, **6**, 46–66.
14 J. van den Bergh, J. Gascon and F. Kapteijn, in *Zeolites and Catalysis*, Wiley-VCH Verlag GmbH & Co. KGaA, 2010, pp. 361–387.
15 J. Perez-Ramirez, C. H. Christensen, K. Egeblad, C. H. Christensen and J. C. Groen, *Chem. Soc. Rev.*, 2008, **37**, 2530–2542.
16 S. Mintova, M. Jaber and V. Valtchev, *Chem. Soc. Rev.*, 2015, **44**, 7207–7233.
17 J. Jiang, J. Yu and A. Corma, *Angew. Chem., Int. Ed.*, 2010, **49**, 3120–3145.
18 V. Valtchev, G. Majano, S. Mintova and J. Perez-Ramirez, *Chem. Soc. Rev.*, 2013, **42**, 263–290.
19 K. Egeblad, C. H. Christensen, M. Kustova and C. H. Christensen, *Chem. Mater.*, 2008, **20**, 946–960.
20 S. Lopez-Orozco, A. Inayat, A. Schwab, T. Selvam and W. Schwieger, *Adv. Mater.*, 2011, **23**, 2602–2615.
21 L. Chen, X. Li, J. C. Rooke, Y. Zhang, X. Yang, Y. Tang, F. Xiao and B. Su, *J. Mater. Chem.*, 2012, **22**, 17381.
22 X. Meng, F. Nawaz and F. Xiao, *Nano Today*, 2009, **4**, 292–301.
23 J. Perez-Ramirez, *Nat. Chem.*, 2012, **4**, 250–251.
24 Y. Yan, X. Guo, Y. Zhang and Y. Tang, *Catal. Sci. Technol.*, 2015, **5**, 772–785.
25 Q. Wang, L. Wang, H. Wang, Z. Li, H. Wu, G. Li, X. Zhang and S. Zhang, *Asia-Pac J. Chem. Eng.*, 2011, **6**, 596–605.
26 K. Y. Lee, H.-J. Chae, S.-Y. Jeong and G. Seo, *Appl. Catal., A*, 2009, **369**, 60–66.
27 W. Schwieger, A. G. Machoke, T. Weissenberger, A. Inayat, T. Selvam, M. Klumpp and A. Inayat, *Chem. Soc. Rev.*, 2016, **45**, 3353–3376.

28 Y. Wei, T. E. Parmentier, K. P. de Jong and J. Zecevic, *Chem. Soc. Rev.*, 2015, **44**, 7234–7261.
29 D. P. Serrano, J. M. Escola and P. Pizarro, *Chem. Soc. Rev.*, 2013, **42**, 4004–4035.
30 I. I. Ivanova and E. E. Knyazeva, *Chem. Soc. Rev.*, 2013, **42**, 3671–3688.
31 Y. Tao, H. Kanoh, L. Abrams and K. Kaneko, *Chem. Rev.*, 2006, **106**, 896–910.
32 F. Xiao and X. Meng, in *Hierarchically Structured Porous Materials*, Wiley-VCH Verlag GmbH & Co. KGaA, 2011, pp. 435–455.
33 V. Valtchev and L. Tosheva, *Chem. Rev.*, 2013, **113**, 6734–6760.
34 S. Mintova, J. P. Gilson and V. Valtchev, *Nanoscale*, 2013, **5**, 6693–6703.
35 S. Teketel, M. W. Erichsen, F. L. Bleken, S. Svelle and K. Petter, *Catalysis*, 2014, **26**, 179–217.
36 M. Stöcker, in *Zeolites and Catalysis*, Wiley-VCH Verlag GmbH & Co. KGaA, 2010, pp. 687–711.
37 W. Song, Y. Wei and Z. Liu, in *Zeolites in Sustainable Chemistry: Synthesis, Characterization and Catalytic Applications*, Springer Berlin Heidelberg, 2016, pp. 299–346.
38 F. H. James and M. M. David, in *Handbook of Zeolite Science and Technology*, CRC Press, 2003.
39 S. Kvisle, T. Fuglerud, S. Kolboe, U. Olsbye, K. P. Lillerud and B. V. Vora, in *Handbook of Heterogeneous Catalysis*, Wiley-VCH Verlag GmbH & Co. KGaA, 2008, pp. 2950–2963.
40 G. T. Vuong and T. O. Do, in *Mesoporous Zeolites: Preparation, Characterization and Applications*, 2015, pp. 79–114.
41 M. Choi, K. Na, J. Kim, Y. Sakamoto, O. Terasaki and R. Ryoo, *Nature*, 2009, **461**, 246–249.
42 S. Askari, A. Bashardoust Siahmard, R. Halladj and S. Miar Alipour, *Powder Technol.*, 2016, **301**, 268–287.
43 M. Razavian, R. Halladj and S. Askari, *Rev. Adv. Mater. Sci.*, 2011, **29**, 83–99.
44 G. A. Tompsett, W. C. Conner and K. S. Yngvesson, *ChemPhysChem*, 2006, **7**, 296–319.
45 F. M. Shalmani, S. Askari and R. Halladj, *Rev. Chem. Eng.*, 2013, **29**, 99–122.
46 X. Meng and F. Xiao, *Chem. Rev.*, 2014, **114**, 1521–1543.
47 H. van Heyden, S. Mintova and T. Bein, *Chem. Mater.*, 2008, **20**, 2956–2963.
48 S. H. Jhung, J.-S. Chang, J. S. Hwang and S.-E. Park, *Microporous Mesoporous Mater.*, 2003, **64**, 33–39.
49 J. W. Jun, J. S. Lee, H. Y. Seok, J.-S. Chang, J.-S. Hwang and S. H. Jhung, *Bull. Korean Chem. Soc.*, 2011, **32**, 1957–1964.
50 S. R. Venna and M. A. Carreon, *J. Mater. Chem.*, 2009, **19**, 3138–3140.
51 S. Lin, J. Li, R. P. Sharma, J. Yu and R. Xu, *Top. Catal.*, 2010, **53**, 1304–1310.
52 G. Yang, Y. Wei, S. Xu, J. Chen, J. Li, Z. Li, J. Yu and R. Xu, *J. Phys. Chem. C*, 2013, **117**, 8214–8222.
53 T. Alvaro-Munoz, C. Márquez-Álvarez and E. Sastre, *Appl. Catal., A*, 2014, **472**, 72–79.
54 T. Alvaro-unoz, E. Sastre and C. Márquez-Álvarez, *Catal. Sci. Technol.*, 2014, **4**, 4330–4339.
55 L. Wu, Z. Liu, L. Xia, M. Qiu, X. Liu, H. Zhu and Y. Sun, *Chin. J. Catal.*, 2013, **34**, 1348–1356.
56 L. Wu, Z. Liu, M. Qiu, C. Yang, L. Xia, X. Liu and Y. Sun, *React. Kinet., Mech. Catal.*, 2014, **111**, 319–334.
57 F. M. Shalmani, R. Halladj and S. Askari, *Powder Technol.*, 2012, **221**, 395–402.
58 Z. Li, J. Martinez-Triguero, P. Concepcion, J. Yu and A. Corma, *Phys. Chem. Chem. Phys.*, 2013, **15**, 14670–14680.
59 S. R. Venna and M. A. Carreon, *J. Phys. Chem. B*, 2008, **112**, 16261–16265.
60 H. Shi, *New J. Chem.*, 2014, **38**, 5276–5278.
61 L. Tosheva and V. P. Valtchev, *Chem. Mater.*, 2005, **17**, 2494–2513.
62 C. Zhang, X. Lu and T. Wang, *J. Energy Chem.*, 2015, **24**, 401–406.
63 E. Koohsaryan and M. Anbia, *Chin. J. Catal.*, 2016, **37**, 447–467.
64 M. Yang, P. Tian, C. Wang, Y. Yuan, Y. Yang, S. Xu, Y. He and Z. Liu, *Chem. Commun.*, 2014, **50**, 1845–1847.
65 Y. Hirota, K. Murata, S. Tanaka, N. Nishiyama, Y. Egashira and K. Ueyama, *Mater. Chem. Phys.*, 2010, **123**, 507–509.
66 S. Askari, Z. Sedighi and R. Halladj, *Microporous Mesoporous Mater.*, 2014, **197**, 229–236.
67 A. Gedanken, *Ultrason. Sonochem.*, 2004, **11**, 47–55.
68 S. Askari and R. Halladj, *Ultrason. Sonochem.*, 2012, **19**, 554–559.
69 S. Askari and R. Halladj, *J. Solid State Chem.*, 2013, **201**, 85–92.
70 M. Dargahi, H. Kazemian, M. Soltanieh, S. Rohani and M. Hosseinpour, *Particuology*, 2011, **9**, 452–457.
71 Y. Rezaei, R. Halladj, S. Askari, A. Tarjomannejad and T. Rezaei, *Particuology*, 2016, **27**, 61–65.
72 Q. Sun, N. Wang, G. Guo and J. Yu, *Chem. Commun.*, 2015, **51**, 16397–16400.
73 Z. Li, J. Martinez-Triguero, J. Yu and A. Corma, *J. Catal.*, 2015, **329**, 379–388.
74 Y.-J. Lee, S.-C. Baek and K.-W. Jun, *Appl. Catal., A*, 2007, **329**, 130–136.
75 N. Nishiyama, M. Kawaguchi, Y. Hirota, D. Van Vu, Y. Egashira and K. Ueyama, *Appl. Catal., A*, 2009, **362**, 193–199.
76 P. Wang, A. Lv, J. Hu, J. A. Xu and G. Lu, *Microporous Mesoporous Mater.*, 2012, **152**, 178–184.
77 H.-J. Chae, I.-J. Park, Y.-H. Song, K.-E. Jeong, C.-U. Kim, C.-H. Shin and S.-Y. Jeong, *J. Nanosci. Nanotechnol.*, 2010, **10**, 195–202.
78 J. H. Park, H. S. Heo, Y.-K. Park, K.-E. Jeong, H.-J. Chae, J. M. Sohn, J.-K. Jeon and S.-S. Kim, *Korean J. Chem. Eng.*, 2010, **27**, 1768–1772.
79 L. Ye, F. Cao, W. Ying, D. Fang and Q. Sun, *J. Porous Mater.*, 2010, **18**, 225–232.
80 M. A. Carreon, S. Li, J. L. Falconer and R. D. Noble, *Adv. Mater.*, 2008, **20**, 729–732.
81 N. Najafi, S. Askari and R. Halladj, *Powder Technol.*, 2014, **254**, 324–330.

82 B. Li, Z. Hu, B. Kong, J. Wang, W. Li, Z. Sun, X. Qian, Y. Yang, W. Shen, H. Xu and D. Zhao, *Chem. Sci.*, 2014, **5**, 1565–1573.
83 D. Verboekend, M. Milina and J. Perez-Ramirez, *Chem. Mater.*, 2014, **26**, 4552–4562.
84 Z. Qin, J.-P. Gilson and V. Valtchev, *Curr. Opin. Chem. Eng.*, 2015, **8**, 1–6.
85 X. Chen, A. Vicente, Z. Qin, V. Ruaux, J. P. Gilson and V. Valtchev, *Chem. Commun.*, 2016, **52**, 3512–3515.
86 X. Chen, D. Xi, Q. Sun, N. Wang, Z. Dai, D. Fan, V. Valtchev and J. Yu, *Microporous Mesoporous Mater.*, 2016, **234**, 401–408.
87 Y. Qiao, M. Yang, B. Gao, L. Wang, P. Tian, S. Xu and Z. Liu, *Chem. Commun.*, 2016, **52**, 5718–5721.
88 S. Abelló, A. Bonilla and J. Pérez-Ramírez, *Appl. Catal., A*, 2009, **364**, 191–198.
89 X. Liu, S. Ren, G. Zeng, G. Liu, P. Wu, G. Wang, X. Chen, Z. Liu and Y. Sun, *RSC Adv.*, 2016, **6**, 28787–28791.
90 S. Ren, G. Liu, X. Wu, X. Chen, M. Wu, G. Zeng, Z. Liu and Y. Sun, *Chin. J. Catal.*, 2017, **38**, 123–130.
91 D. Xi, Q. Sun, J. Xu, M. Cho, H. S. Cho, S. Asahina, Y. Li, F. Deng, O. Terasaki and J. Yu, *J. Mater. Chem. A*, 2014, **2**, 17994–18004.
92 F. Schmidt, S. Paasch, E. Brunner and S. Kaskel, *Microporous Mesoporous Mater.*, 2012, **164**, 214–221.
93 J.-W. Jun, J. Jeon, C.-U. Kim, K.-E. Jeong, S.-Y. Jeong and S.-H. Jhung, *J. Nanosci. Nanotechnol.*, 2013, **13**, 2782–2788.
94 S. Rimaz, R. Halladj and S. Askari, *J. Colloid Interface Sci.*, 2016, **464**, 137–146.
95 J. Yao, Y. Huang and H. Wang, *J. Mater. Chem.*, 2010, **20**, 9827–9831.
96 X. Meng and F. Xiao, in *Mesoporous Zeolites: Preparation, Characterization and Applications*, 2015, pp. 199–226.
97 Y. Cui, Q. Zhang, J. He, Y. Wang and F. Wei, *Particuology*, 2013, **11**, 468–474.
98 M. Razavian and S. Fatemi, *Z. Anorg. Allg. Chem*, 2014, **640**, 1855–1859.
99 H. Yang, X. Liu, G. Lu and Y. Wang, *Microporous Mesoporous Mater.*, 2016, **225**, 144–153.
100 Q. Sun, N. Wang, G. Guo, X. Chen and J. Yu, *J. Mater. Chem. A*, 2015, **3**, 19783–19789.
101 F. Wang, L. Sun, C. Chen, Z. Chen, Z. Zhang, G. Wei and X. Jiang, *RSC Adv.*, 2014, **4**, 46093–46096.
102 J. Zheng, W. Zhang, Z. Liu, Q. Huo, K. Zhu, X. Zhou and W. Yuan, *Microporous Mesoporous Mater.*, 2016, **225**, 74–87.
103 Q. Zhang, S. Liu and S. Yu, *J. Mater. Chem.*, 2009, **19**, 191–207.
104 H. Cölfen and M. Antonietti, *Angew. Chem., Int. Ed.*, 2005, **44**, 5576–5591.
105 F. Wang, V. N. Richards, S. P. Shields and W. E. Buhro, *Chem. Mater.*, 2014, **26**, 5–21.
106 L. Kong, B. Shen, Z. Jiang, J. Zhao and J. Liu, *React. Kinet., Mech. Catal.*, 2015, **114**, 697–710.
107 M. Choi, H. S. Cho, R. Srivastava, C. Venkatesan, D. H. Choi and R. Ryoo, *Nat. Mater.*, 2006, **5**, 718–723.
108 D. P. Serrano and P. Pizarro, in *Mesoporous Zeolites: Preparation, Characterization and Applications*, 2015, pp. 157–198.
109 B. Yang, P. Zhao, J. Ma and R. Li, *Chem. Phys. Lett.*, 2016, **665**, 59–63.
110 L. Chen, R. Wang, S. Ding, B. Liu, H. Xia, Z. Zhang and S. Qiu, *Chem. J. Chin. Univ.*, 2010, 1693–1696.
111 S.-T. Yang, J.-Y. Kim, H.-J. Chae, M. Kim, S.-Y. Jeong and W.-S. Ahn, *Mater. Res. Bull.*, 2012, **47**, 3888–3892.
112 L. Wu and E. J. M. Hensen, *Catal. Today*, 2014, **235**, 160–168.
113 H. Sharifi Pajaie and M. Taghizadeh, *React. Kinet., Mech. Catal.*, 2016, **118**, 701–717.
114 Q. Sun, N. Wang, D. Xi, M. Yang and J. Yu, *Chem. Commun.*, 2014, **50**, 6502–6505.
115 C. Jo, J. Jung, H. S. Shin, J. Kim and R. Ryoo, *Angew. Chem.*, 2013, **125**, 10198–10201.
116 C. Wang, M. Yang, P. Tian, S. Xu, Y. Yang, D. Wang, Y. Yuan and Z. Liu, *J. Mater. Chem. A*, 2015, **3**, 5608–5616.
117 C. Wang, M. Yang, M. Li, S. Xu, Y. Yang, P. Tian and Z. Liu, *Chem. Commun.*, 2016, **52**, 6463–6466.
118 C. Wang, M. Yang, W. Zhang, X. Su, S. Xu, P. Tian and Z. Liu, *RSC Adv.*, 2016, **6**, 47864–47872.
119 Y. Jin, Q. Sun, G. Qi, C. Yang, J. Xu, F. Chen, X. Meng, F. Deng and F. Xiao, *Angew. Chem., Int. Ed.*, 2013, **52**, 9172–9175.
120 P. Wu, M. Yang, W. Zhang, S. Xu, P. Guo, P. Tian and Z. Liu, *Chem. Commun.*, 2017, **53**, 4985–4988.
121 C. Pagis, A. R. Morgado Prates, D. Farrusseng, N. Bats and A. Tuel, *Chem. Mater.*, 2016, **28**, 5205–5223.
122 M. E. Davis, *Chem. Mater.*, 2014, **26**, 239–245.
123 K. G. Strohmaier, in *Zeolites and Catalysis*, Wiley-VCH Verlag GmbH & Co. KGaA, 2010, pp. 57–86.
124 Y. Liu, L. Wang and J. Zhang, *Mater. Lett.*, 2011, **65**, 2209–2212.
125 J. Gong, F. Tong, X. Ji, C. Zeng, C. Wang, Y. Lv and L. Zhang, *Cryst. Growth Des.*, 2014, **14**, 3857–3863.
126 Y. Li, Y. Huang, J. Guo, M. Zhang, D. Wang, F. Wei and Y. Wang, *Catal. Today*, 2014, **233**, 2–7.
127 J. Liu and J. Yu, in *Zeolites and Zeolite-Like Materials*, Elsevier, 2016, pp. 1–32.
128 D. Xi, Q. Sun, X. Chen, N. Wang and J. Yu, *Chem. Commun.*, 2015, **51**, 11987–11989.
129 W. J. Roth, B. Gil, W. Makowski, B. Marszalek and P. Eliasova, *Chem. Soc. Rev.*, 2016, **45**, 3400–3438.
130 J. Gong, C. Wang, C. Zeng and L. Zhang, *Microporous Mesoporous Mater.*, 2016, **221**, 128–136.
131 X. Meng, L. Wang and F. Xiao, in *Zeolites in Sustainable Chemistry: Synthesis, Characterization and Catalytic Applications*, Springer Berlin Heidelberg, 2016, pp. 3–35.
132 R. A. Sheldon, *Green Chem.*, 2007, **9**, 1273–1283.
133 Y. Wang and F. Xiao, *Chem. Rec.*, 2016, **16**, 1054–1066.
134 Q. Sun, N. Wang, R. Bai, X. Chen and J. Yu, *J. Mater. Chem. A*, 2016, **4**, 14978–14982.
135 J. Zhu, Y. Cui, Y. Wang and F. Wei, *Chem. Commun.*, 2009, 3282–3284.

136 H. Yang, Z. Liu, H. Gao and Z. Xie, *J. Mater. Chem.*, 2010, **20**, 3227–3231.
137 M. Milina, S. Mitchell, P. Crivelli, D. Cooke and J. Perez-Ramirez, *Nat. Commun.*, 2014, **5**, 3922.
138 K. A. Cychosz, R. Guillet-Nicolas, J. Garcia-Martinez and M. Thommes, *Chem. Soc. Rev.*, 2017, **46**, 389–414.
139 B. Coasne, *New J. Chem.*, 2016, **40**, 4078–4094.
140 L. Zhang, A. N. C. van Laak, P. E. de Jongh and K. P. de Jong, in *Zeolites and Catalysis*, Wiley-VCH Verlag GmbH & Co. KGaA, 2010, pp. 237–282.
141 H. Friedrich, P. E. de Jongh, A. J. Verkleij and K. P. de Jong, *Chem. Rev.*, 2009, **109**, 1613–1629.
142 Q. Sun, Y. Ma, N. Wang, X. Li, D. Xi, J. Xu, F. Deng, K. B. Yoon, P. Oleynikov, O. Terasaki and J. Yu, *J. Mater. Chem. A*, 2014, **2**, 17828–17839.
143 K. P. de Jong, A. J. Koster, A. H. Janssen and U. Ziese, in *Studies in Surface Science and Catalysis*, Elsevier, 2005, vol. 157, pp. 225–242.
144 W. Wan, C. Xiao and X. Zou, in *Mesoporous Zeolites: Preparation, Characterization and Applications*, 2015, pp. 425–460.